Vessel correspondence in pre-post-intervention DSA images of ischemic stroke patients

by

Michael Angelo Berrospi

to obtain the degree of Master of Science in Biomedical Engineering
at the Delft University of Technology to be defended on October 2nd, 2024 at 10:00.

Supervisors:
Dr. F.M. Vos, Erasmus MC, TU Delft
Dr. T. van Walsum, Erasmus MC
F. te Nijenhuis, Erasmus MC
Dr. R. Su, Erasmus MC

Project duration: February 15, 2024 - October 2, 2024

Thesis committee:		
	Dr. F.M Vos, chair	Erasmus MC, TU Delft
	Dr. T. van Walsum	Erasmus MC
	Dr. Q. Tao	TU Delft

TU Delft Delft University of Technology

Erasmus MC Universitair Medisch Centrum Rotterdam

Vessel correspondence in pre-post-intervention DSA images of ischemic stroke patients

Michael Angelo Berrospi

September 18, 2024

Abstract

Ischemic stroke, a leading cause of death and disability worldwide, occurs when a blood vessel is occluded by a thrombus. Current therapies for ischemic stroke, include Intravenous thrombolysis (IVT) and Endovascular thrombectomy (EVT). EVT relies on a Thrombolysis in Cerebral Infarction (TICI) score for assessing treatment effectiveness. This score, based on the visual evaluation of medical images by physicians, suffers from inter- and intra-observer variability, as it is influenced by the individual rater's judgment. Digital Subtraction Angiography (DSA) imaging is commonly utilized both before therapy to identify the occluded vessel and after therapy to evaluate the treatment outcome. Accurate vessel correspondence before and after treatment is crucial for a reliable assessment. To enhance current evaluation methods and address this challenging task, we propose two automated approaches for determining vessel correspondence in pre- and post-EVT DSA imaging. The proposed methods utilize graphical representations of the cerebral vascular network and distinct matching procedures. We refer to the methods as **r**egistration-**b**ased **v**essel **m**atching (**RB-VM**) and **g**raph **b**ased vessel matching (**GB-VM**). The methods were evaluated using manually annotated data with the RB-VM and GB-VM methods achieving a recall of 82.7% (78.2; 85.7) and 51.3% (47.4; 54.4) respectively. This work marks a significant step towards automatic stroke therapy assessment and showcases the potential benefits of graph based algorithms for this task, paving the way for more reliable and objective treatment assessments.

Abbreviations

EVT	Endovascular Thrombectomy
TICI	Thrombolysis in Cerebral Infarction
DSA	Digital Subtraction Angiography
GM	Graph Matching
MinIP	Minimum Intensity Projection

I. Introduction

Stroke is considered a major contributor to death and disability worldwide. Mortality following an acute stroke was nearly 10% preceding the use of modern therapy procedures such as Intravenous Thrombolysis (IVT) and Endovascular Thrombectomy (EVT) [1]. Despite the development of new advanced methods, stroke remains the second leading cause of death and the third leading cause of death and disability combined globally. In 2019, ischemic stroke was recorded to account for 62.4% of all cases [2, 3, 4]. Notably, this type of stroke is known to cause neurological death and long-term disability, which in turn places significant health and economic burdens on society [4]. This highlights the importance of developing effective therapy procedures, as well as effective techniques to evaluate their success.

The current EVT therapy assessment procedures include visual evaluation of medical images by physicians and the use of revascularization scores known as Thrombolysis in Cerebral Infarction (TICI). Specifically, TICI scores are commonly used as a technical outcome measure following EVT procedures, and their different levels define the extent of brain reperfusion [5, 6]. There have been multiple TICI versions due to the variability in the different scale definitions with the latest being eTICI [6] and autoTICI [5]. The autoTICI score aimed to improve several limitations of existing TICI scores. An important drawback of the TICI scores is inter- and intra-observer variation since the scoring is subject to various factors such as the rater. Similarly to autoTICI, we aim to mitigate the shortcomings of the currently used TICI scores and propose an alternative way to assess the outcome of EVT procedures.

During ischemic stroke treatment, a thrombus, also known as a blood clot, which causes vessel blockage is removed from the affected vessel. Digital Subtraction Angiography (DSA) imaging is commonly performed prior to the treatment to identify the blocked vessel and following treatment to assess the outcome. DSA provides a means of visualizing blood flow dynamics and changes in vasculature appearance over time making it optimal for the treatment evaluation. A substantial factor when determining the treatment outcome quality is identifying vessels that appear and disappear after the treatment.

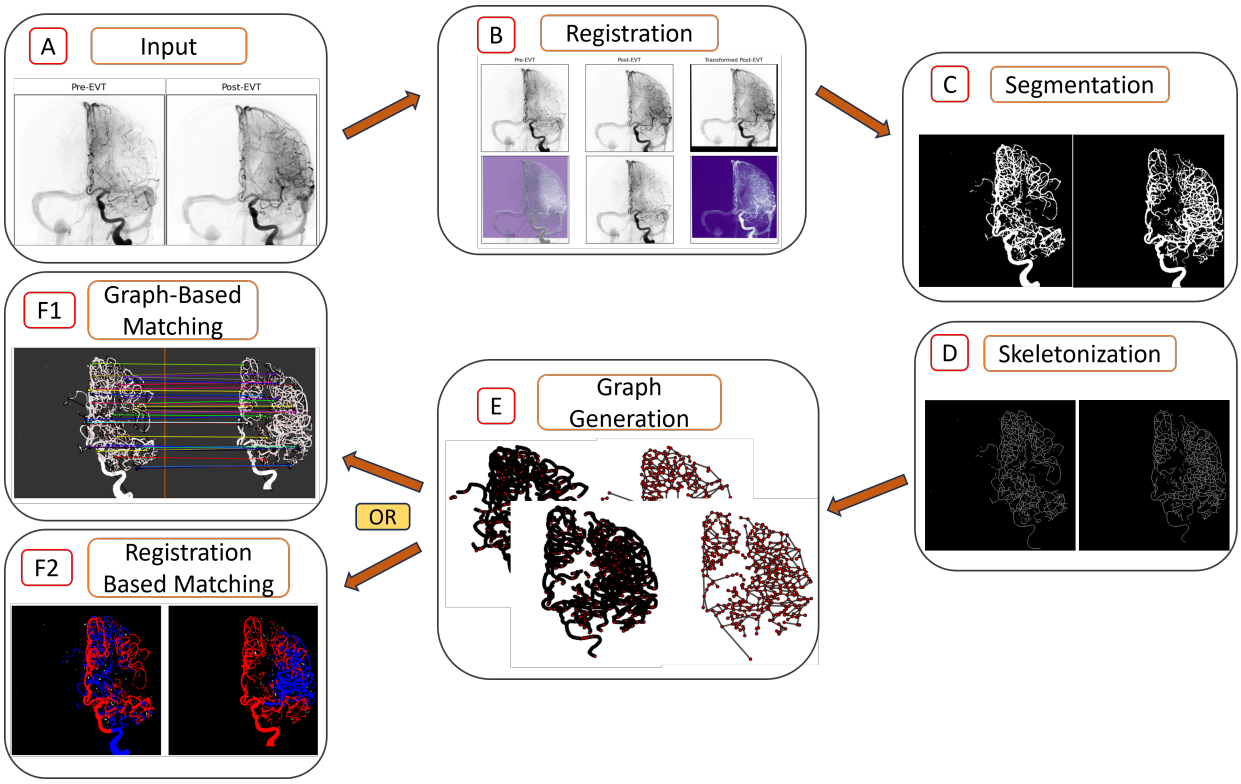

Fig. 1. Pipeline of the proposed registration-based (RB-VM) and graph-based (GB-VM) vessel matching. (A) Minimum Intensity Projections (MinIP) extracted from pre and post-EVT DSA sequences. (B) Registration of the MinIP images using the Scale-Invariant Feature Transformation (SIFT) [7] method. (C) Arterial segmentations of pre and post-EVT DSA sequences using the Temporal UNet segmentation model used in [8]. (D) Centerline extraction or skeletonization of the generated segmentations. (E) Graph generation using the segmentation skeletons, including multiple simplification layers and node and edge feature extraction. The left and right images correspond to the initial and final simplified graph respectively. The red circles and black lines represent the vertices and edges of the graphs respectively. (F1) Node correspondence between the generated graphs. Graph nodes represent bifurcation or vessel connection points. (F2) Segmentation matches produced where the red and blue segments represent the matched and unmatched segments respectively.

This information helps physicians ascertain if the therapy was successful.

To address this challenging task, we aimed to develop a graph based matching algorithm that detects vessel correspondences between pre and post-EVT DSA imaging. Graph matching (GM) is a classic and long studied computational problem that aims to find an optimal correspondence (matching) between vertices in two or more graphs. It has been applied successfully across various fields and areas including but not limited to, pattern recognition, computer vision, bio-informatics and social networks [9, 10, 11].

We hypothesized that a graphical representation of the brain vasculature combined with graph matching could provide additional insight regarding the vessel correspondence. Graph structures can naturally represent a multitude of real world data and brain vasculature can be considered, as vessels appear to be a collection of trees. Recent studies focusing on vessel analysis and visualization support this notion. They also note how graphical representation of medical structures could be beneficial [12, 13, 14, 15, 16, 17]. Rist et al. [18] make use of vessel graph representation to achieve vessel labeling in stroke patients for specific main arteries present in the Circle of Willis. Moriconi et al. [19] employ graph matching on brain vessels for vascular network alignment or registration. Yao et al. [20] utilize graph matching to identify the aorta and pulmonary artery and achieve segmentation. Riffaud et al. [21] apply graph matching to abdominal aortic segmentations for branch detection and artery identification.

Recent developments in deep learning have introduced alternative ways to solve graph based problems. Namely, Graph Neural Networks (GNNs) are a type of neural network specifically designed to deal with graph representations. In the realm of vessel related medical imaging, multiple works utilize these new developments for vessel classification [15], bifurcation detection [22] and artery semantic labelling [23, 24, 25]. These works share a similar notion of extracting visual descriptors or node features from a Convolutional Neural Network (CNN) used previously for vessel segmentation. The

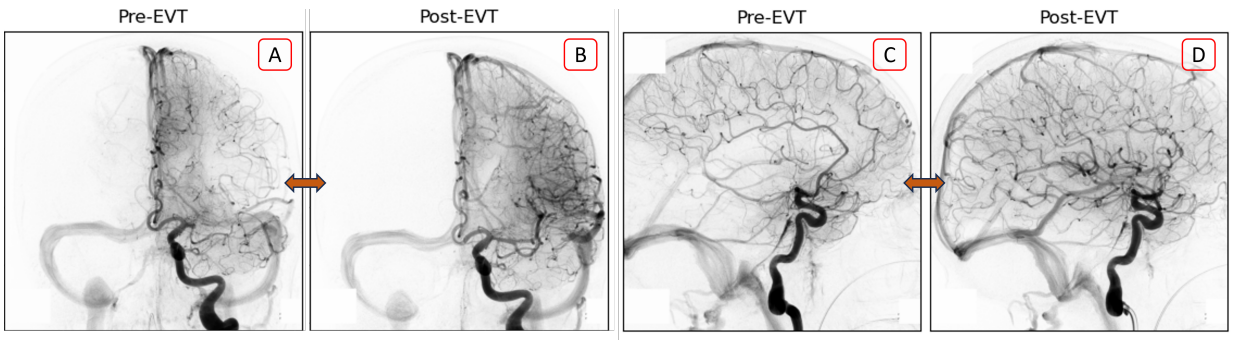

Fig. 2. Pre and post MinIP pairs extracted from input DSA series. They present Anterior-Posterior (AP) (A-B) and Lateral (C-D) orientations.

use of these visual descriptors is well established and has been used frequently and successfully in computer vision, as is demonstrated in the well known SuperGlue [26] model.

With all previous work in mind, we developed and assessed two main methods of determining vessel correspondence in pre and post-EVT DSA imaging. For the remainder of this work we shall refer to them as **r**egistration-**b**ased **v**essel **m**atching (**RB-VM**) and **g**raph **b**ased vessel matching (**GB-VM**). These methods aim to produce correspondences automatically by employing a graphical representation of the cerebral vascular network and matching procedures as outlined in Figure 1. To the best of our knowledge, this is the first attempt to calculating correspondence between complete brain vascular networks.

This work is structured as follows. Section II outlines the methodologies employed to achieve our goal and Section III provides insight on the data used and data preprocessing. Section IV contains the results and performance evaluation of the developed methods. Lastly, Section V and Section VI conclude this work by discussing the findings, limitations of the methods and possible future developments.

II. Methods

A. Problem Definition

We are given DSA imaging of patients that have undergone an EVT procedure following a stroke incident, both before and after the procedure. The goal is to determine correspondence between the pre and post-intervention vessels. This allows the comparison of vessels with no correspondence. These include pre-intervention vessels which may have disappeared due to new occlusions, and post-intervention vessels which signify areas that have been recanalized. The comparisons can provide additional insight on the success of the procedure.

B. Initial Registration

The RB-VM and GB-VM methods use nearly identical processes until the final matching stage. First, an initial registration method was used based on the assumption that better aligned inputs would benefit the matchings. The registration was performed using Minimum Intensity Projection (MinIP) images extracted from the pre and post DSA series illustrated in Figure 2. It consists of three steps. First, keypoints with their respective scale-invariant feature descriptors are calculated according to the SIFT method proposed by Lowe et al. [7]. Following the keypoint localization and feature descriptor calculations, a match between keypoints is determined using the Euclidean distance (ED) between their feature descriptors. The validity of matched points is determined using a ratio between the closest and second closest Euclidean distances as described by Lowe et al. [7]. Lastly, the matched keypoints are used to calculate a transformation (homography) matrix which is used to perform a perspective transformation on the post-EVT image. The calculation of the transformation matrix utilizes the Random Sample Consensus (RANSAC) method to detect outliers in the matches and discard them [27].

Following the transformation of the post-EVT image, the quality of the registration, in other words the alignment between the pre-post images, is evaluated using the Mutual Information (MI) score. MI is described by the following equation:

$$I(X;Y) = \sum_{x \in X} \sum_{y \in Y} p(x,y) \log \frac{p(x,y)}{p(x)p(y)} \tag{1}$$

$p(x,y)$: Joint Probability Mass Function

$p(x)$: Marginal Probability Mass Function of X

$p(y)$: Marginal Probability Mass Function of Y

In this case, the probability mass functions are calculated by creating a bi-dimensional histogram of the images and converting the bin counts to probability values. We opted for this to deal with cases where the

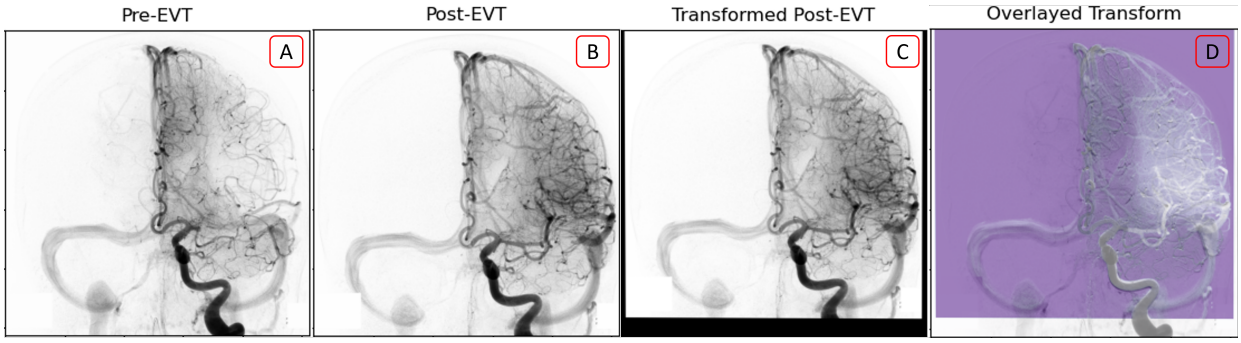

Fig. 3. Example registration of pre and post MinIP DSA series. (A-B) Pre-Post EVT MinIP images. (C) Registered post-EVT image. (D) Registered post-EVT image overlayed on the pre-EVT image. Gray areas are interpreted as overlapping structures and white areas as non-overlapping.

registration did not improve alignment. The alignment was considered improved if the MI was increased after transformation. Otherwise, the initial unregistered images were used.

C. Segmentation

Vascular segmentation of the DSA series was an essential step in developing our methods. The Temporal UNet model proposed by Su et al. [8] was used to extract venous and arterial segmentations. In more detail, the model takes DSA series inputs and produces venous and arterial segmentation masks. The segmentation model architecture is provided in Figure 5 and an example of arterial segmentations can be seen in Figure 4. The produced methods only made use of the arterial segmentations. This choice was based on the clinical importance of the vessels. MinIP based vessel segmentations, via a traditional UNet model, produced several segmentations with dense vessels which made them quite hard to distinguish as can be seen in the Appendix A, Figure 12. The use of MinIP segmentations or the combination of arteries and veins greatly complicates the subsequent steps and served as an additional factor for the choice of arterial segmentations.

D. Centerline Extraction

Centerlines are the basis for creating the graphs. In order to create the centerlines we applied skeletonization, also known as thinning, to the vessel segmentations. An illustration of said centerlines can be seen in Figure 4. Multiple skeletonization techniques exist. We chose to use the method proposed by Lee et al. [28], based on a visual evaluation of the produced skeletons as it produced comparatively few erroneous branch point extensions. The centerline extraction procedure also produces the Eucliden Distance Transform (EDT) matrix which

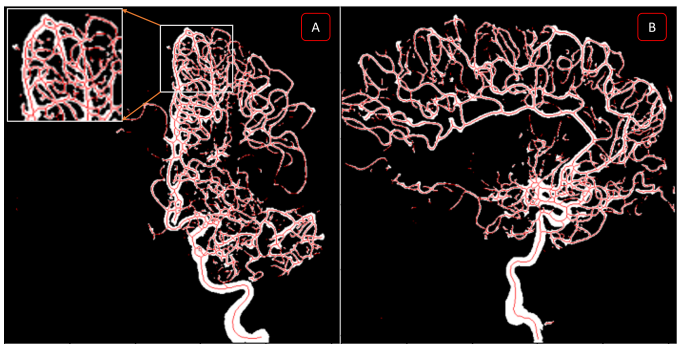

Fig. 4. Illustration of anterior-posterior (AP) (A) and lateral (B) segmentations along with their skeletonizations displayed as red one pixel wide lines.

contains the distances to the nearest boundary pixel for every segmented pixel. Its functionality is highlighted in Sections II-E and II-G.

Algorithm 1 Graph Generation

Input: Centerlines, EDT

1: Create vertices located at centerline points
2: Add coordinates and radius attributes to vertices
3: Connect neighboring vertices via edges
4: Apply class 1, 2 and isolated segment filters
5: Perform Graph Feature Extraction (Section II-E2)
6: Perform major graph simplification (Section II-E2)
7: Apply class 1+ and 2+ filters

Output: Simplified graph with vertex and edge features

E. Graph Generation

The graph generation process was greatly inspired by the work of Bumgarner et al. [12]. Below we first discuss the graph generation and simplification, after which we examine the graph feature extraction.

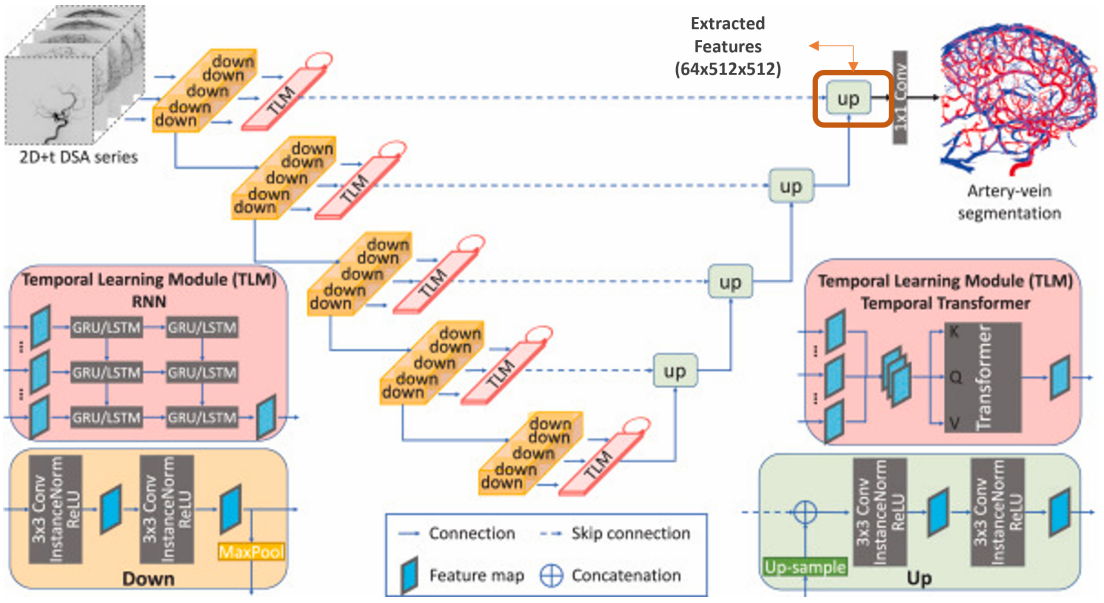

Fig. 5. Network architecture for artery–vein segmentation in DSA series proposed by Su et al. [8]. The features maps used in the first type of main feature extraction are extracted from the final up-convolution layer of the model and are highlighted in the figure.

1) ***Graph Generation and Simplification*** The initial full graph consists of vertices located at each centerline point extracted from the centerline extraction step. Every vertex is assigned two attributes; coordinates and radius. The radius attribute is determined during the centerline extraction process via the EDT. EDT refers to calculating the Euclidean distance (ED) from the centerline point to the center of the nearest non-vessel neighbor point in the segmented mask.

Following the vertex creation, an 8-neighborhood area is scanned to determine the node connectivity and edges connecting neighboring vertices are generated. Loops and multiedges are then removed to prevent duplicate edges. It is essential to mention that vertices are characterized as bifurcation or connection points if they have more than 2 connecting neighbors. This notion is used throughout the graph simplification process. For the remainder of this work, we will refer to them as bifurcation points.

This initial generated graph results in a vertex count in the thousands. Such a large number of vertices would render the GB-VM method infeasible. Therefore, multiple simplification steps were taken. First, class 1 and 2 filters, as described by Bumgarner et al. [12], were utilized. The purpose of these filters was to eliminate clusters, also known as cliques, of bifurcation points. Specifically, the class 1 filter targets maximal cliques with 3 or 4 bifurcation points, whereas class 2 targets clusters between 5 and 50 bifurcation points. Next, isolated vessel segments were identified and removed based on a predefined length. The mentioned simplification steps allowed us distinguish between bifurcation points, endpoints and vessel segment points by the vertex degree count n_d, which was $n_d > 2$, $n_d = 1$ and $n_d = 2$ respectively.

The next simplifications are applied after the processes mentioned in Section II-E2, but are outlined here to maintain consistency. They are separate as these simplifications were designed to simplify the graphs following the significant reduction mentioned in Section II-E2. Adding to the already extensive work of Bumgarner et al. [12], we devised two additional simplification processes. We refer to them as class 1+ and class 2+ filters. Class 1+ simplifies bifurcation point clusters if the distance between their nodes is under a defined threshold. Class 2+ complements this by targeting and simplifying segments formed by bifurcation nodes whose distance between nodes falls under a certain threshold. The thresholds for both filters were determined empirically. When vertices are merged, we assign the average coordinates and radius as the new vertex features. The external edges connected to the vertices prior to simplification are connected to the new vertex and maintain their original features. In the case of duplicate external connections, the segment with the largest length is kept. Examples of class 1+ and 2+ filters are provided in Figure 6. These two filters are used iteratively until no further simplifications can be performed.

2) ***Graph Feature Extraction*** The extraction of features from the graphs was performed after the first simplification steps proposed by Bumgarner et al. [12]. Vessel segments were identified by filtering out all non-

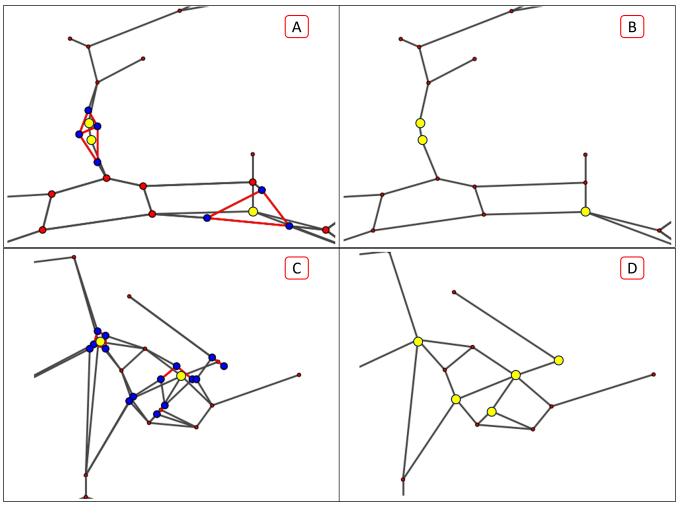

Fig. 6. Class 1+ and 2+ filters. (A)-(C) correspond to the graphs before being filtered while (B)-(D) represent the filtered graphs. (A)-(B) and (C)-(D) depict the class 1+ and class 2+ filters respectively. The blue circles denote the targeted points while the red lines connected to them represent their respective edges which are then removed. The nodes are combined and form new nodes shown in yellow, maintaining the original external edges.

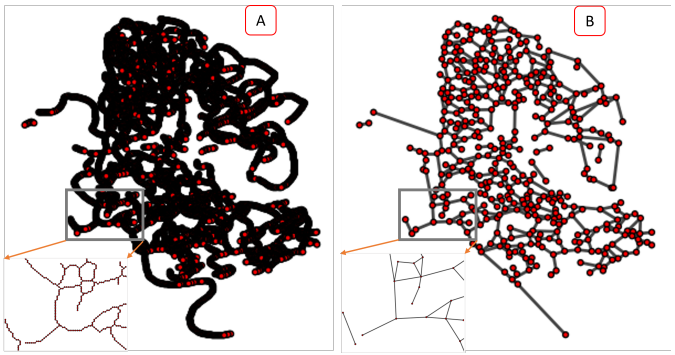

Fig. 7. Examples of original (A) and simplified (B) graphs where vertices are represented by red circles and edges as black lines connecting them.

vessel segment points (i.e. $n_d \neq 2$) and then sorting through the remaining individual components. For each identified segment, the mean, minimum, maximum, and standard deviation of the segment radius were calculated. Next, the segment length was calculated using a smooth path constructed through B-splines. The length was approximated using ED calculations between a defined number of points along the spline identified using the Cox-De Boor algorithm. The use of B-splines prevented irregular paths that did not reflect the vessel shape accurately and produced more reliable length measures [12]. Finally, tortuosity measurements were computed by finding the arc-cord ratio of the segment, which was calculated by dividing the segment length by the ED between the start and end points. Tortuosity was used as a measure reflecting the bending of the vessel segment.

With the identification of segments and their end-points, the graph underwent a major reduction. After the reduction, only the bifurcation nodes were maintained along with the edges connecting them, as these are of primary interest. The extracted vessel segment features were added as edge attributes. The significance of the graph size reduction can be seen in Figure 7 as the node count is reduced from thousands to hundreds.

F. Feature Extraction

In order to determine corresponding nodes, feature values are used in the matching process. There are two types of features: image-based (i.e. independent of the graph), and graph-based (i.e. representing intrinsic properties of nodes and edges). As such, this section focuses on the image-based features and we refer to the graph-based in Section II-E. We have experimented with two types of feature extraction methods.

*1) **UNet Feature Maps.*** The UNet based feature extraction method is directly related to the segmentation model. In more detail, 64 feature maps are extracted from the final up-convolution layer of the segmentation model as displayed in Figure 5. This extraction layer was chosen based on the hypothesis that the GB-VM methods would benefit from feature maps that make use of both high and low level features. This is a defining property of features generated by the contracting and expansive UNet architecture paired with the use of skip connections. The feature maps of the post-EVT imaging were transformed using the calculated transformation matrix mentioned in Section II-B. Visualization of a feature map for a DSA sequence is provided in Appendix A, Figure 13.

*2) **Leung-Malik (LM) Filter Bank Feature Maps.*** This feature extraction method utilizes Leung-Malik filter banks [29] to generate and extract the required features. The LM set is a multi scale, multi orientation filter bank with 48 filters. It consists of first and second derivatives of Gaussians at 6 orientations and 3 scales making a total of 36; 8 Laplacian of Gaussian (LOG) filters; and 4 Gaussians. The filters occur at the basic scales $\sigma = [\sqrt{2}, 2, 2\sqrt{2}, 4]$. The first and second derivative filters occur at the first three scales with an elongation factor of 3 (i.e. $\sigma_x = \sigma$ and $\sigma_y = 3\sigma_x$). The Gaussians occur at the four basic scales while the 8 LOG filters occur at σ and 3σ. The filter bank and a generated feature map are shown in Appendix A, Figure 14 and Figure 15 respectively.

G. RB-VM Approach

The RB-VM vessel correspondence utilizes the majority of processes seen in Figure 1 with some distinctions. The registration, segmentation and skeletonization processes are applied as described in their respective sections. The graph creation is nearly identical. However, only the initial group of simplifications mentioned in Section II-E1 were applied. Namely, class 1 and 2 filters and isolated segment removal. Next, vessel identification was performed as described in Section II-E2. This was then used in tandem with the previously calculated skeletons and segmentations to create a labeled mask of all segments in the graphs. Specifically, centerline pixels were labeled based on the segment they were a part of resulting in a labeled skeleton. The watershed algorithm [30] was then applied, utilizing the labeled skeletons, the EDT, and the arterial segmentations. Example labeled segmentations are provided in Figure 8.

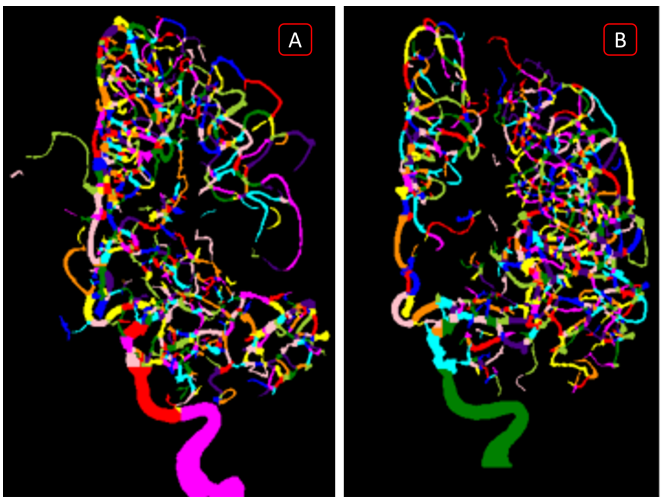

Fig. 8. Labeled vessel segmentation mask. (A)-(B) depict the pre-post labeled segmentation masks respectively. Each segment is characterized by a different color.

The correspondence was then calculated in two steps. First, a pixel-wise method utilizing the segmentations was used. Segmented pixels present in both pre and post procedure segmentations were considered to be matched. The matching procedure is performed scanning a 7×7 square region of interest centered at the corresponding pixel in the other image, and assigning the closest segmented pixel if any were present. This allows close neighbouring matches and was performed on all segmented pixels in the pre EVT image. Lastly, to attain the final vessel correspondence, the labeled segment masks and the matched segmented pixels were combined. A vessel segment was considered to have a corresponding vessel in the other image when the number of matched segmented pixels exceeded the non-segmented ones. An additional figure (Figure 16) providing further clarification of the proposed procedures is given in Appendix A.

H. GB-VM Approaches

The GB-VM approaches are shown in Figure 1. We implemented three different versions that differ in how they apply feature matching. These are GB-VM-Patched (GB-VM-P), GB-VM-Single-Scale (GB-VM-SS) and GB-VM-Multi-Scale (GB-VM-MS).

These methods are inspired by the GM combinatorial problem. GM is a computational problem that aims to find an optimal correspondence between vertices in two or more graphs. This can be achieved by maximizing their node and edge affinities. In this case, the vertices represent the vessel bifurcations or connection points. One way to achieve this correspondence is through feature matching. This approach is demonstrated in the well known SuperGlue [26] model which served as a form of inspiration. Feature matching refers to finding correspondences between pairs of vertices by taking into account the affinity of their respective feature vectors $f_i^{G_1}, \forall i \in G_1$ and $f_j^{G_2}, \forall i \in G_2$, where G_1, G_2 represent the pre-post graphs respectively.

In order to determine correspondence between pre-post graph vertices we considered the vertex-to-vertex affinities. A vertex-to-vertex correspondence can be represented by an assignment matrix $M \in \{0,1\}^{n_1 \times n_2}$ where n_1 and n_2 represent the number of pre-post graph nodes respectively. As described by Sarlin et al. [26], the assignment matrix M can be obtained by computing a similarity matrix $S \in \Re^{n_1 \times n_2}$ for all possible matches and maximizing the total score $\sum_{i,j} S_{i,j} M_{i,j}$ under the constraints that $M^T 1_{n_1} \leq 1_{n_2}$ and $M 1_{n_2} = 1_{n_1}$. This formulation is analogous to solving a linear assignment problem. The vertex-wise similarity is computed using the inner product as described by the equation:

$$S_{i,j} =< f_i^{G_1}, f_j^{G_2} >, \forall (i,j) \in G_1 \times G_2 \qquad (2)$$

where $< .,. >$ denotes the inner product, and G_1, G_2 represent the pre-post graphs respectively.

The linear assignment problem discussed above can be solved successfully using the Hungarian algorithm. Classically used for bipartite graph matching [26], the algorithm iteratively normalizes rows and columns of the similarity matrix S until a solution is reached.

The matching procedure followed by these approaches was as follows. Vertex feature vectors were created utilizing the UNet or LM feature maps (See Section II-F) and a defined neighborhood size. The feature vectors contained 64 and 48 features for UNet and LM-Filter Bank feature maps respectively. A defined neighborhood

was used to combine feature map responses from a wider area rather than the sole pixel/vertex of interest. The hypothesis was that this would improve the descriptiveness of vertex features by considering neighboring responses. The extracted vertex features were then combined with the graph vertex attributes (described in Section II-E1), namely, the vertex coordinates and radius. These steps resulted in a feature vector, with a length dependent on the features used, for each vertex in the examined pre-post graphs. Combinations of the feature map and graph generated features were experimented with to determine their importance. Next, using the computed feature vectors, the vertex-wise similarity matrix S is calculated. The Hungarian algorithm provided by the Pygmtools library (version 0.5.2) [31] was then applied to obtain a doubly-stochastic assignment matrix. The Hungarian algorithm was originally designed to work with square matrices. As such, S was padded in the case where $n_1 \neq n_2$. The resulting assignment matrix M was used draw the matching nodes as can be seen in Figure 11.

To reduce cluttering, matched vertices were connected if the ED between them was under a threshold. It offers similar functionality to a filter, where unlikely or outlier matches are filtered out. This assumption is only valid in the case where the initial registration is successful or if the vessels are well aligned prior to the registration. Otherwise, true matches may exceed the threshold and be filtered out resulting in a misleading visualization.

The three approaches,GB-VM-P, GB-VM-SS and GB-VM-MS, are mainly distinguished by how the feature matching is performed. In more detail, GB-VM-SS used the so called single-scale graphs which were the pre-post graphs created via the graph generation step. GB-VM-MS divided the graphs into multiple subgraphs based on different vessel radii scales followed by an iterative matching procedure. A radius scale refers to a range of radii (e.g. between 3 and 5) where included vertices and their edges generate new subgraphs. Lastly, GB-VM-P, as the name suggests, split the original segmentation images into patches, allowing for a more localized approach. The patch size was set to 128×128 which split the original 512×512 segmentations into 16 patches. In the case of GB-VM-MS and GB-VM-P the complete matching was achieved iteratively by combining the intermediate matches. For the GM-VM-MS method, intermediate matches refer to matches obtained on the different scale graphs. On the other hand, for the GM-VM-P method intermediate matches are matches obtained from individual patches.

III. Data

In this work, we used a subset of the MR CLEAN Registry [32] dataset for developing and evaluating the proposed methods. The MR CLEAN Registry is a multicenter registry which contains patients residing in the Netherlands that suffered acute ischemic stroke and underwent EVT between March 2014 and December 2018 [32]. The DSA series included in the registry contain anterior–posterior (AP) or lateral views (Figure 2) and were acquired using various imaging systems (e.g., Philips, GE, and Siemens). Specifically, our original dataset included the first 50 patients present in the MR CLEAN Registry (Part 1 & 2). These were extracted from a larger dataset of 2000 patients including patients with pre- and post-EVT DSA series. Given the use of the segmentation pipeline presented by Su et al. [8], a similar data selection and preprocessing procedure was followed.

A. Data Selection

First, DSA series missing time information were excluded. The final number of patients following the selection process was 47 with a total number of 164 DSA series.

B. Data Preprocessing

The DSA series had varying lengths and were shortened to a maximum of 20 frames. Moreover, we linearly resampled the temporal resolution of the series to 1 fps and normalized the intensity values to be in the range of [0,255]. Following these steps, MinIP images were extracted from the selected and processed DSA series. Two additional preprocessing steps preceded the registration of MinIP images. First, the extracted MinIP images contained text about imaging attributes near the corners of the image. This text was removed using contouring followed by masking of the areas. Moreover, a number of images contained black borders at given boundaries which were also removed. These steps were taken to prevent the registration being affected by these artifacts as it was greatly affected if not applied, as demonstrated in Appendix A, Figure 17 and Figure 18.

C. Data Annotation

The annotations used for evaluating both proposed methods were created by the authors using a web-based graph matching annotation tool built in-house available at: GM Annotation Tool. The images used to create annotations consisted of corresponding patches including the arterial segmentations along with their respective

skeletons. As visualized in Figure 9, the annotations result in a list of bifurcation or vessel connection points between corresponding pre and post-EVT DSA arterial segmentation patches. The complete interface of the annotation tool is provided in Appendix A, Figure 19.

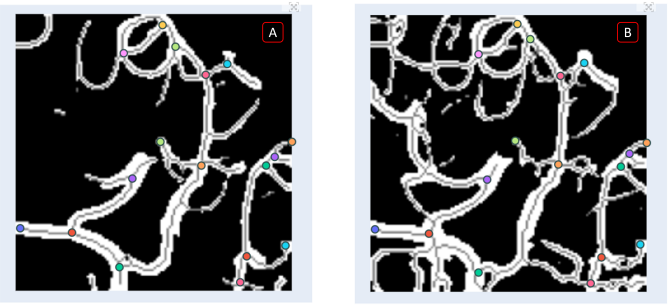

Fig. 9. Annotations used as ground truth for evaluating the proposed methods. The images correspond to the pre (A) and post-EVT (B) patches respectively. The patched images include the arterial segmentations with their respective skeletons. The matching points in the two images have identical colors and mark bifurcation or vessel connection points that exist before and after the intervention.

During the generation of these annotations, the dataset was further refined. Initially, 2 random patches were extracted per patient orientation (AP or Lateral) to increase variability. The patches were randomly sampled from the 16 128×128 patches generated from the original segmentations. The total number of patches extracted was 328 which translates to 164 pairs of pre-post patches. The number of pairs is equal to the number of DSA series used. Upon visual inspection of the collected patches, multiple patches were either replaced or the entire DSA series was discarded. The patches were judged based on the criteria mentioned in Table I. Patches were replaced when identification of matching bifurcations was too challenging. On the other hand, DSA series were discarded when registration failed and the initial alignment was subpar. In addition, they were discarded when the segmentation quality was insufficient or when the registration failed but was undetected by the MI score. The cases where DSA series were discarded due to bad registration are considered failures of the RB-VM method. The series discarded due to the rest of the criteria are considered failures for both the RB-VM and GB-VM methods. Finally, the evaluation dataset consisted of 35 patients with a total of 119 DSA series and 238 patches or 119 pairs.

IV. Experiments and Results

The proposed GB-VM methods depend on several parameters. These include the feature maps used (UNet or LM Filter Bank), the neighborhood size used to extract features from the feature maps, the combination of vertex features used and lastly the type of normalization applied to the features. All method performances were assessed, with additional experiments exploring the impact of the parameters mentioned above on the GB-VM methods. All performances are reported in Table III.

A. Evaluation Metrics

The methods were assessed using the manually annotated correspondences mentioned in Section III. They are evaluated in terms of their sensitivity (Recall) defined by the following:

$$Sensitivity(Recall) = \frac{TP}{TP + FN} \tag{3}$$

where TP and FN are True Positive and False Negative respectively. The meaning of TP and FN were different depending on the method. In the context of the RB-VM method, a TP match was considered when a pair of matching annotated points were present in the matched segments identified by the method. FN matches were all the annotated points that were not part of an identified matched segment. On the other hand, in the case of GB-VM methods, a TP exists when a pair of annotated points is correctly matched and is FN otherwise. The annotations create a point (pixel) correspondence, which is likely not exactly reproduced by the GB-VM methods. We therefore consider matches by the method that are in a neighbourhood around the annotations and evaluate the vertices present in that neighborhood. If no vertices are present, the annotation is overlooked. We do not consider False Positive (FP) and True Negative (TN) metrics. Given that our annotations were incomplete and imperfect, when considering the number of vertices present in the graphs, these values would not offer any meaningful insights.

95% confidence intervals were calculated for the recall metric via bootstrap resampling of the evaluation data. Specifically, random samples were selected with replacement from the annotated patches 20 times and the recall metric was calculated for these sets. The 95% confidence

TABLE I
Series removal criteria during annotations.

Criteria (# of removals)
Bad SIFT registration and bad initial alignment (9)
Challenging identification of matching bifurcations (3)
Bad SIFT registration undetected by MI score (7)
Faulty text or border removal (1)
Segmentation of insufficient quality (7)

TABLE II
Resulting metrics for all initial experiments. The optimal parameters are used for every subsequent experiment except the case of feature normalization where the features used are only LM features. Bold values indicate the best performing parameter per experiment and underlined values indicate the best performing method.

Experiment	**Parameter**	**Recall (%)**		
		GB-VM Patched (GB-VM-P)	GB-VM Single-Scale (GB-VM-SS)	GB-VM Multi-Scale (GB-VM-MS)
# Neighbors	3 (8-neighboring pixels)	46.3	**42.3**	**45.6**
	5 (24-neighboring pixels)	**<u>47.4</u>**	41.1	43.0
	7 (48-neighboring pixels)	46.2	36.7	40.9
	9 (80-neighboring pixels)	44.7	34.5	39.3
Features Used	LM Features	47.4	42.3	**45.6**
	LM Features + Coordinates	**<u>51.5</u>**	43.3	40.3
	LM Features + Radius	47.3	42.3	45.3
	LM Features + Coordinates + Radius	51.5	**43.4**	40.6
Feature Normalization	None	**<u>47.4</u>**	**42.3**	**45.6**
	Z-score Standardization (Instance)	47.1	41.4	45.3
	Min-Max Normalization (Instance)	43.1	35.2	34.9
	Z-score Standardization (Distribution)	46.1	40.0	43.3
	Min-Max Normalization (Distribution)	39.6	29.4	30.3

intervals were computed using the percentile method by finding the 2.5th and 97.5th percentile of the calculated values. The performance of the algorithms given varying parameters was considered significantly different when their recall metrics did not coincide within their 95% confidence intervals.

Additionally, the computational efficiency of methods was recorded. The time was calculated as the average time required to produce matchings per patient over all the data used during the evaluations.

Regarding the GB-VM approaches, initial experiments were performed to assess their performance. These experiments report on the recall metric calculated on the evaluation dataset without the use of bootstrap resampling and 95% confidence intervals, to limit the computational time needed to a feasible amount. As shown in the initial results supplied in Table II, the GB-VM-P method outperformed both GB-VM-SS and GB-VM-MS and was thus selected for subsequent evaluations.

B. Implementation

The proposed methods have multiple parameters which are outlined in this section.

For the registration, we utilized the SIFT, homography matrix calculation and perspective transformation implementations provided by the OpenCV library (version 4.8.1) [33]. RANSAC was used during the homography matrix calculation with a reprojection threshold of 5 and maximum iterations set to 2000 (default).

The skeletonization and watershed algorithm implementations provided by the scikit-image package (version 0.22.0) [34] were used for centerline extraction and to create the labeled arterial segmentations.

During the feature extraction using the LM filter banks, the feature maps were calculated by applying the filters on the MinIP image. To achieve this, both the MinIP images and the filters were transformed to the frequency domain. Next, Fast Fourier Transform (FFT) was used to get the frequency response followed by the Inverse FFT (IFFT) to convert our data back to the spatial domain. This approach was preferred compared to the spatial convolution alternative as the execution time was reduced by a factor of $\simeq 40$.

The graph generation process was performed using an isolated vessel segment filter length of 10, class 1+ vertex distance threshold of 10 and class 2+ distance threshold of 4. The length in this case refers to the number of pixels or vertices that make up the segment and distance refers to the maximum pixel distance between vertices.

Four radii scales were used when experimenting with the GB-VM-MS method [(0-2), (2-3), (3-4), 4]. Each scale refers to vessels having a minimum and maximum radius (e.g. (min=0-max=2)).

Lastly, for the visualization of the GB-VM methods, the ED threshold used when plotting matched vertices was set to 15 ($\simeq 10$ pixels)

C. RB-VM Results

The performance of the RB-VM method is shown at the top of Table III. The calculated recall was 82.7% (78.2; 85.7).

TABLE III
Resulting metrics for all experiments. The recall is given with its 95% confidence intervals. Bold values indicate the best performing parameter per experiment.

Method	Experiment	Parameter	Recall (%)
RB-VM	-	-	**82.7 (78.2; 85.7)**[a]
GB-VM Patched (GB-VM-P)	Feature map	Temporal UNet	9.7 (7.3; 11.7)
		LM Filter Bank	**47.5 (43.4; 51.0)**
	# Neighbors	3 (8-neighboring pixels)	46.2 (42.7; 49.3)
		5 (24-neighboring pixels)	47.5 (43.4; 51.0)
		7 (48-neighboring pixels)	45.8 (41.8; 49.7)
		9 (80-neighboring pixels)	44.4 (39.8; 47.3)
	Features used	LM Features	47.5 (43.4; 51.0)
		LM Features + Coordinates	51.3 (47.4; 54.3)
		LM Features + Radius	47.3 (43.3; 50.1)
		LM Features + Coordinates + Radius	51.3 (47.4; 54.3)
	Feature Normalization	None	47.5 (43.4; 51.0)
		Z-score Standardization (Instance)	47.4 (42.2; 51.4)
		Min-Max Normalization (Instance)	43.5 (38.2; 48.0)
		Z-score Standardization (Distribution)	46.3 (42.0; 49.9)
		Min-Max Normalization (Distribution)	40.1 (34.5; 45.6)

[a] Metric is computed different to the rest, and a direct quantitative comparison can not be made.

D. Experiment 1: Feature Maps

The performance using both UNet and LM filter bank feature maps was compared to identify the best approach. The recall results are presented in Table III. The other parameters were set to the following values. We set the neighborhood size to 5, used only the features extracted from the feature maps, and did not apply any feature normalization.

The performance was significantly improved when using the LM filter bank features compared to the Temporal UNet features with a recall of 47.5% (43.4;51.0) and 9.7% (7.3;11.7) respectively. Considering the results, the remaining experiments were performed using the LM filter bank feature maps.

In terms of computational efficiency, UNet and LM filter bank feature maps took on average 7.2s and 1.7s respectively. The GB-VM-P method computation time was determined on an individual patch basis which was not representative of a complete patient. To account for this, we provide an expected time per patient of 4.4s. This was calculated based on the assumption that 12 out of 16 total patches include vessels on average. The patches with no vessels present were not processed.

E. Experiment 2: Number of Neighbors

To investigate the effect of different size neighborhoods used during feature extraction, four neighborhood sizes were explored; 3, 5, 7, 9. The sizes refer to the size (in pixels) of the square ROI from which the features were sampled and their performance is displayed in Table III. Similarly to the first experiment, we only used the LM features and did not apply any feature normalization.

While the different neighborhoods do not have a statistically significant performance difference, on average the neighborhood size of 5 performed slightly better than the rest with a recall of 47.5% (43.4; 51.0). Consequently, a neighborhood of 5 was selected as the optimal choice.

Computational efficiency is similar to the one mentioned in Section IV-D with a slight increase of $\approx$ 1s as the neighborhood size increases.

F. Experiment 3: Features used

In order to gain insight into the added value of the graph-extracted features for the matching, combinations of all features were considered. We use a neighborhood size of 5. The neighborhood size was chosen based on the optimal value determined from Experiment 2. Feature normalization was not applied to maintain consistency across the experiments. However, additional insightful experiments regarding its effect with relation to the features used are provided in Appendix B. The performance measures are presented in Table III.

The metrics suggest that the inclusion of the coordinates as features improve the average performance. However, the results for LM features and LM features plus coordinates are comparable, as the metrics fall within each other's 95% confidence interval. Similarly, the inclusion of coordinate features outperforms the radius features with recalls of 51.3% (47.4 ; 54.3) and 47.3% (43.3; 50.1) respectively but is not statistically significant. It is noteworthy that, the inclusion of radius features leads to slightly reduced performance compared to only using the LM features. When both coordinates and radius features are included the results are identical to solely including the coordinates.

G. Experiment 4: Feature Normalization

The effect of feature normalization was tested by normalizing the features using two different approaches: Z-score standardization and min-max normalization. The type of normalization was further divided into instance and distribution based. Instance based refers to calculating the normalization parameters (mean, standard deviation, minimum, maximum) per instance, whereas distribution based indicates a calculation using the entire dataset. For these experiments the optimal choice from experiment 2 (neighborhood size of 5) was used. Moreover, solely the LM features were used. Additional experiments exploring the effect of normalization with regards to the features used are provided in Appendix B.

Interestingly, significant mean differences can be seen between the non-normalized and min-max distribution based normalization performance with 47.5% (43.4; 51.0) and 40.1% (34.5; 45.6) respectively, but their performance is comparable according to the 95% confidence intervals. The instance based min-max normalization's performance is also substantially reduced but is not statistically significant. On the other hand, z-score normalization's performance is comparable to the non-normalized with the distribution based only slightly lacking with a recall of 46.3% (42.0; 49.9). It is noticeable that the instance based normalization's average performance is improved compared to the distribution based.

V. Discussion

In this section, we briefly discuss the methods used to find correspondences, their limitations and possible future research.

A. General

Determining the success of interventional procedures following ischemic stroke is a critical step in the therapy of patients. The current assessment procedures rely on visual evaluation of medical imaging and are accompanied by several shortcomings such as intra-observer variability. To overcome the limitations, we proposed two automated methods which aim to identify vessel correspondences between pre-post procedure DSA imaging. The methods are able to produce informative visualizations and may assist clinicians in making well-informed decisions.

The RB-VM methods resulted in a recall of 82.7% (78.2; 85.7) and no parameter experimentation was performed. The best performing GB-VM method was GB-VM-P with the best performing experiment achieving a recall of 51.3% (47.4; 54.3).

Notably, the performance was substantially improved when using LM features instead of Temporal UNet features. We hypothesize that this was due to the inherent nature of the features and what their original purpose was. Since they were extracted from a layer of a deep learning segmentation model, it is likely that the feature maps were steered towards identifying vascular segments. While this was ideal for the segmentation model, the extracted features were likely not descriptive enough for the task at hand. On the other hand, the features generated from the LM filter banks seem to be more distinctive and allow for increased bifurcation matchings and improved performance.

In terms of neighborhood size, for the GB-VM-P method the optimal was found to be 5. This indicates that while taking more neighboring pixels into account when calculating the features was beneficial, including too many neighbors was counter-productive. One possible interpretation could be that adding too many neighbors leads to more generalized features and decreases the descriptiveness of individual points.

It is noteworthy that the inclusion of radius features slightly reduces the performance of GB-VM methods. However, it is not statistically significant. A possible explanation, is the radial difference between matching vertices caused from imaging, segmentation and skeletonization discrepancies. To elaborate, the contrast flow may differ between pre-post EVT imaging. As a result, matching vessels may appear to have different diameters. In addition, segmentation and skeletonization errors may also influence vessel diameters. Therefore, this could be an indication that the inclusion of radius features is not optimal. In addition, we observe that when both coordinates and radius features are included the results are identical to solely including the coordinates. This can be considered evidence of the greater coordinate features influence on the final outcome.

With regards to the feature normalization experiments,

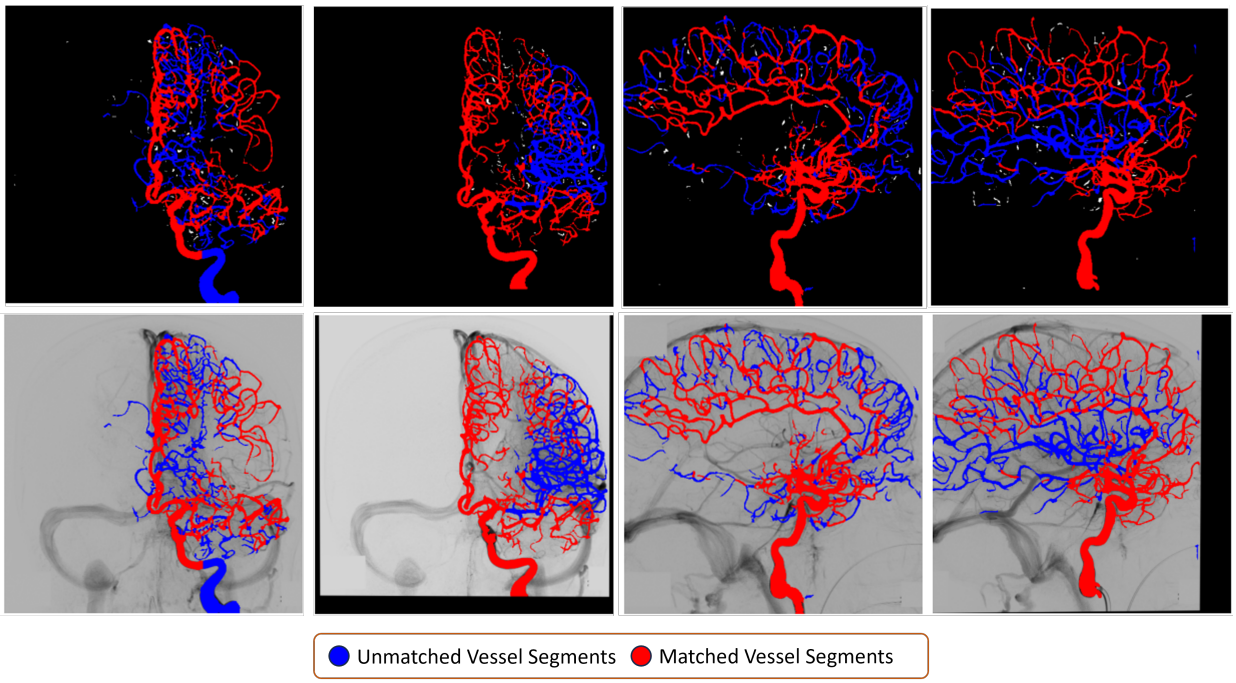

Fig. 10. Example results from the RB-VM method. The first row depict the pre- and post-EVT masked arterial matches. The second row depicts the matched vessels on the original MinIP DSA images. Corresponding vessels are shown in red and missing or new vessels are displayed in blue.

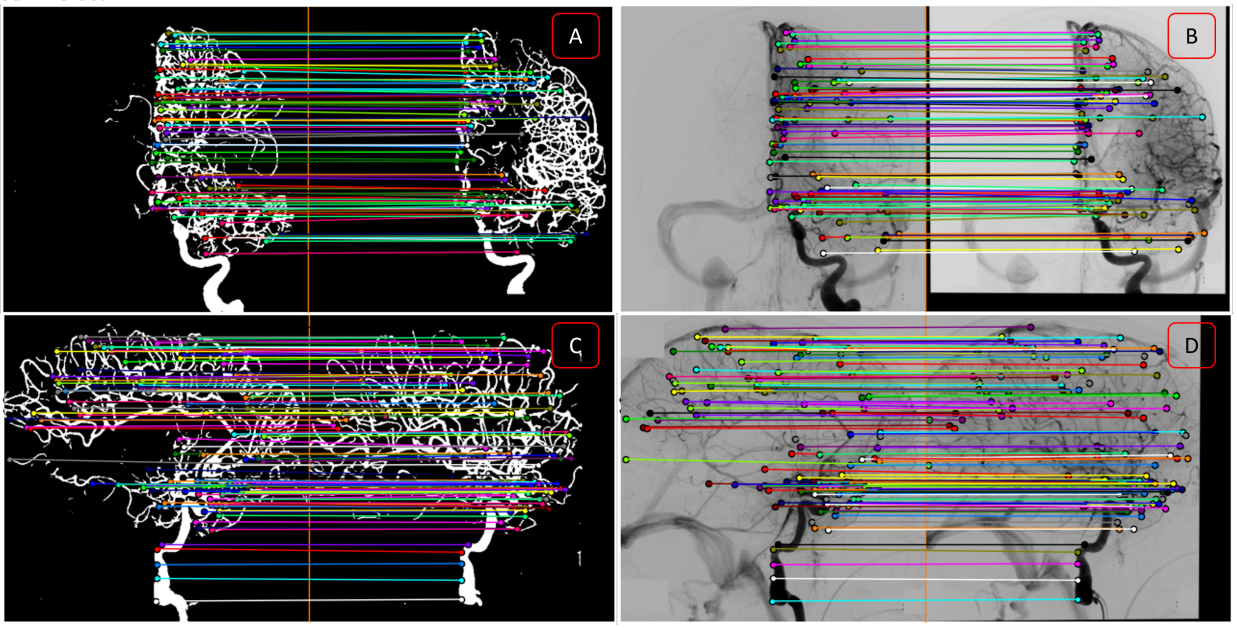

Fig. 11. Example results from the GB-VM-P method. Matches on AP (A-B) and lateral (C-D) orientations displayed on the arterial segmentations (A & C) and on the MinIPs (B & D). Left and right images are pre and post EVT respectively.

we notice improved average performance with the use of instance based normalization compared to distribution based. A possible explanation for this could be a kind of bias correction per instance. By bias correction we refer to correcting differences in the mean of feature values.

The additional experiments exploring the effect of normalization with relation to the features used (Table IV) suggest that z-score normalization tends to outperform min-max normalization in both instance and distribution based cases. Additionally, when combining LM features and coordinates or radius, z-score normalization improves both GB-VM-SS and MS methods but has little effect on the GB-VM-P method.

A notable limitation of the RB-VM method is its dependence on the quality of the registration. If not successful, the performance is expected to reduce significantly since the method is primarily based on the spatial location of the vessels. The GB-VM methods were developed as a means to combat this limitation and allow vessel matching regardless of the vessel positions.

Furthermore, the GB-VM methods produce a matching between points in the pre-post EVT imaging but they lack in creating a visual vessel identification similar to the RB-VM method. The GB-VM methods could be enhanced by generating matching vessels using a heuristic approach that considers sets of paired vessel endpoints. Such an approach could also give rise to an alternative evaluation method more suited to the RB-VM method, allowing for a more fitting and reliable comparison.

Moreover, we hypothesized that the MI score would be sufficient to detect unsuccessful registrations. However, during the visual evaluation performed during the annotation process, multiple cases were detected where the MI score failed. A potential cause for this could be significant projection distortions reflecting the non-ideal transformation matrix. These distortions might cause misleading MI scores. One way to mitigate this limitation could be to include an additional measure, such as a maximum projection threshold, resembling a two-factor evaluation of the registration quality. Alternatively, a more direct approach would be to let clinicians assess the registration and only then consider the final results.

It is important to mention that while registration is included in the pipeline of GB-VM methods, it is not actually necessary. It was utilized in our case as the evaluation data was generated using the registered images and annotating badly registered patches would be extremely difficult. In addition, we hypothesized that registered images paired with the use of coordinate features could elevate matching performance. However, when the coordinate features are not used, registration is not necessary. In this case, the feature matching is independent of the spatial location of vertices. This property is a significant distinction between the RB-VM and GB-VM methods. Conversely, the matched points can be used to register pre-post images, similarly to how the SIFT registration is performed. The ability to register images based on matching bifurcations or vessel connections may pave the way to improved vascular brain imaging registration that is unaffected by additional artifacts. Such a procedure could simultaneously register the images and provide insight into new, missing and matched vascular segments.

B. Limitations

With respect to the RB-VM evaluation, it is important to acknowledge the performance inflation compared to the GB-VM methods. The results might be overestimated since the testing data was originally created to evaluate the GB-VM method and later adapted for both. While the GB-VM methods require an exact match between points, the RB-VM evaluation considers a greater area which greatly increases the chances of correct matches. This design choice did not allow for a valid comparison between the RB- and GB-VM methods.

In relation to GB-VM methods, we note that the performance increase when using coordinate features might be biased and may require a successful registration prior to the calculation. As such, we suggest the coordinate features only be used when successful registration is performed beforehand.

C. Future Research

A multitude of ways could be used to enhance our work. First we focus on potential ways to improve the current work and then we explore alternative methods to solve the problem.

With regards to the RB-VM method, we chose a registration technique using SIFT as a baseline. Evaluating the performance of the registration was outside the scope of our research. However, empirically, the registration tends to fail occasionally. This is demonstrated by the number of data excluded during the annotation process discussed in Section III. We propose that alternative registration methods with increased robustness and accuracy can benefit and improve this method.

Furthermore, the points used as vertices are not only bifurcation points but also vessel connection points created by projections from the original X-Ray imaging. The algorithms could benefit from a bifurcation detection algorithm [16, 21, 22]. That could potentially simplify

the problem by removing unwanted vertices and therefore improve matching performance. Similarly, including the segment pruning proposed by Bumgarner et al. [12] in the graph generation process can remove additional vertices (and edges) simplifying the problem further.

Additionally, in the case of feature extraction via LM filter banks, the features are not scale or rotationally invariant. While the filters include multiple scales and orientations, the extracted features are not inherently invariant. An alternative would be to use a different feature extraction method, such as Schmid or Maximum Response (MRS4) filter banks, which generate rotational and/or scale invariant features [35].

In addition, different ways to calculate the similarity of feature vectors could be used. In our experiments, we focused on using the inner product. Even though the inner product provides a quantitative measure of similarity the methods may benefit from different measures. Alternatively, cosine similarity or feature vector euclidean distances are plausible choices. Cosine similarity is the inner product normalized by the vectors' L2 norms and has been used widely in natural language processing applications [36]. This type of similarity focuses on the angular alignment of vectors whereas the inner product also takes their magnitude into account.

Moreover, graph connectivity and structure could play vital roles in identifying matching vessels. The structural information can be considered if modern techniques such as GNNs are used. In more detail, GNNs can integrate structural information via their message passing capabilities. In short, message passing is a technique that iteratively aggregates features from connected vertices. As a result, the features of individual vertices are influenced by their neighbors introducing additional structural information. This can be done in both supervised and unsupervised ways. One example could be to use the GraphSAGE [37] model with an unsupervised loss function. With a sufficient amount of good quality ground truth data, supervised learning techniques that learn how to produce the assignment matrix could also be used [38, 39, 40, 41]. Importantly, acquiring good quality ground truth data is very expensive time-wise and in the case of vessel segments may even be considered impractical. Wang et al. [42] proposed achieving a matching using discrepancy minimization between traditional graph matching techniques and a trainable model. Utilizing such a technique could be something worth exploring further for our current application.

VI. Conclusions

In this study, we explored two approaches that detect vessel correspondences between pre and post-EVT DSA imaging. Our goal was to enhance the current post procedural assessment following ischemic stroke therapy. It marks a significant step towards stroke therapy assessment with minimized inter- and intra-observer variation. The RB-VM method achieved a recall of 82.7% (78.2; 85.7) followed by the best performing GB-VM method with 51.3% (47.4; 54.3). Our methods serve as examples of how graph based algorithms can be utilized for stroke therapy evaluation and should be explored further.

References

[1] T. F. Hasan *et al.*, "Overview of Acute Ischemic Stroke Evaluation and Management," *Biomedicines*, vol. 9, no. 10, 2021. DOI: 10.3390/biomedicines9101486.

[2] V. L. Feigin *et al.*, "World Stroke Organization (WSO): Global Stroke Fact Sheet 2022," *International Journal of Stroke*, vol. 17, no. 1, pp. 18–29, 2022. DOI: 10.1177/17474930211065917.

[3] V. L. Feigin *et al.*, "Global, regional, and national burden of stroke and its risk factors, 1990–2019: a systematic analysis for the Global Burden of Disease Study 2019," *The Lancet Neurology*, vol. 20, no. 10, pp. 795–820, 2021. DOI: 10.1016/S1474-4422(21)00252-0.

[4] L. Pu *et al.*, "Projected Global Trends in Ischemic Stroke Incidence, Deaths and Disability-Adjusted Life Years From 2020 to 2030," *Stroke*, vol. 54, no. 5, pp. 1330–1339, 2023. DOI: 10.1161/STROKEAHA.122.040073.

[5] R. Su *et al.*, "autoTICI: Automatic Brain Tissue Reperfusion Scoring on 2D DSA Images of Acute Ischemic Stroke Patients," *IEEE Transactions on Medical Imaging*, vol. 40, no. 9, pp. 2380–2391, 2021. DOI: 10.1109/TMI.2021.3077113.

[6] D. S. Liebeskind *et al.*, "ETICI reperfusion: Defining success in endovascular stroke therapy," *Journal of NeuroInterventional Surgery*, vol. 11, no. 5, pp. 433–438, 2019. DOI: 10.1136/neurintsurg-2018-014127.

[7] D. G. Lowe, "Distinctive Image Features from Scale-Invariant Keypoints," *International Journal of Computer Vision*, 2004.

[8] R. Su *et al.*, "CAVE: Cerebral artery–vein segmentation in digital subtraction angiography," *Computerized Medical Imaging and Graphics*, vol. 115, 2024. DOI: 10.1016/j.compmedimag.2024.102392.

[9] M. Fey *et al.*, "Deep Graph Matching Consensus," 2020.

[10] J. Yan *et al.*, "A short survey of recent advances in graph matching," in *ICMR 2016 - Proceedings of the 2016 ACM International Conference on Multimedia Retrieval*, 2016, pp. 167–174. DOI: 10.1145/2911996.2912035.

[11] C. Oyarzun Laura *et al.*, "Graph matching survey for medical imaging: On the way to deep learning," *Methods*, vol. 202, pp. 3–13, 2022. DOI: https://doi.org/10.1016/j.ymeth.2021.06.008.

[12] J. R. Bumgarner and R. J. Nelson, "Open-source analysis and visualization of segmented vasculature datasets with VesselVio," *Cell Reports Methods*, vol. 2, no. 4, 2022. DOI: 10.1016/j.crmeth.2022.100189.

[13] J. C. Paetzold *et al.*, "Whole brain vessel graphs: a dataset and benchmark for graph learning and neuroscience (vesselgraph)," *arXiv preprint arXiv:2108.13233*, 2021. DOI: https://doi.org/10.48550/arXiv.2108.13233.

[14] C. Prabhakar *et al.*, "Vesselformer: Towards Complete 3D Vessel Graph Generation from Images," Tech. Rep., 2023, pp. 320–331.

[15] S. Mishra *et al.*, "VTG-Net: A CNN Based Vessel Topology Graph Network for Retinal Artery/Vein Classification," *Frontiers in Medicine*, vol. 8, 2021. DOI: 10.3389/fmed.2021.750396.

[16] S. S. Patankar and J. V. Kulkarni, "Orthogonal moments for determining correspondence between vessel bifurcations for retinal image registration," *Computer Methods and Programs in Biomedicine*, vol. 119, no. 3, pp. 121–141, 2015. DOI: 10.1016/j.cmpb.2015.02.009.

[17] X. Guo *et al.*, "Statistical Shape Analysis of Brain Arterial Networks (BAN)," 2022.

[18] L. Rist *et al.*, "Bifurcation matching for consistent cerebral vessel labeling in CTA of stroke patients," *International Journal of Computer Assisted Radiology and Surgery*, vol. 18, no. 3, pp. 509–516, 2023. DOI: 10.1007/s11548-022-02750-9.

[19] S. Moriconi *et al.*, "Elastic Registration of Geodesic Vascular Graphs," 2018. DOI: 10.1007/978-3-030-00928-1_91.

[20] Z. Yao *et al.*, "Graph matching and deep neural networks based whole heart and great vessel segmentation in congenital heart disease," *Scientific Reports*, vol. 13, no. 1, 2023. DOI: 10.1038/s41598-023-34013-1.

[21] S. Riffaud *et al.*, "Automatic branch detection of the arterial system from abdominal aortic segmentation," *Medical and Biological Engineering and Computing*, vol. 60, no. 9, pp. 2639–2654, 2022. DOI: 10.1007/s11517-022-02603-2.

[22] G. Wang *et al.*, "Automatic vessel crossing and bifurcation detection based on multi-attention network vessel segmentation and directed graph search," *Computers in Biology and Medicine*, vol. 155, 2023. DOI: 10.1016/j.compbiomed.2023.106647.

[23] C. Zhao *et al.*, "EAGMN: Coronary artery semantic labeling using edge attention graph matching network," *Computers in Biology and Medicine*, vol. 166, 2023. DOI: 10.1016/j.compbiomed.2023.107469.

[24] C. Zhao *et al.*, "Hyper Association Graph Matching with Uncertainty Quantification for Coronary Artery Semantic Labeling," 2023.

[25] C. Zhao *et al.*, "AGMN: Association graph-based graph matching network for coronary artery semantic labeling on invasive coronary angiograms," *Pattern Recognition*, vol. 143, 2023. DOI: 10.1016/j.patcog.2023.109789.

[26] P.-E. Sarlin *et al.*, "SuperGlue: Learning Feature Matching with Graph Neural Networks," Tech. Rep.

[27] M. A. Fischler and R. C. Bolles, "Graphics and Image Processing Random Sample Consensus: A Paradigm for Model Fitting with Apphcatlons to Image Analysis and Automated Cartography," Tech. Rep., 1981.

[28] T.-C. Lee, "Building Skeleton Models via 3-D Medial Surface/Axis Thinning Algorithms," 1994.

[29] T. Leung and J. Malik, "Representing and Recognizing the Visual Appearance of Materials using Three-dimensional Textons," Tech. Rep. 1, 2001, pp. 29–44.

[30] R. Barnes *et al.*, "Priority-flood: An optimal depression-filling and watershed-labeling algorithm for digital elevation models," *Computers and Geosciences*, vol. 62, pp. 117–127, 2014. DOI: 10.1016/j.cageo.2013.04.024.

[31] R. Wang *et al.*, "Pygmtools: A Python Graph Matching Toolkit," Tech. Rep., 2024, pp. 1–7.

[32] I. G. Jansen *et al.*, "Endovascular treatment for acute ischaemic stroke in routine clinical practice: Prospective, observational cohort study (MR CLEAN Registry)," *BMJ (Online)*, vol. 360, 2018. DOI: 10.1136/bmj.k949.

[33] G. Bradski, "The OpenCV Library," *Dr. Dobb's Journal of Software Tools*, 2000.

[34] S. van der Walt *et al.*, "scikit-image: image processing in Python," *PeerJ*, vol. 2, e453, 2014. DOI: 10.7717/peerj.453.

[35] M. Varma and A. Zisserman, "A Statistical Approach to Texture Classification from Single Images," Tech. Rep.

[36] R. Navigli and F. Martelli, *An overview of word and sense similarity*, 2019. DOI: 10 . 1017 / S1351324919000305.

[37] W. L. Hamilton *et al.*, "Inductive Representation Learning on Large Graphs," 2017.

[38] R. Wang *et al.*, "Neural Graph Matching Network: Learning Lawler's Quadratic Assignment Problem with Extension to Hypergraph and Multiple-graph Matching," 2021.

[39] A. Nowak *et al.*, "Revised Note on Learning Quadratic Assignment with Graph Neural Networks," in *2018 IEEE Data Science Workshop, DSW 2018 - Proceedings*, 2018, pp. 229–233. DOI: 10.1109/DSW.2018.8439919.

[40] R. Wang *et al.*, "Combinatorial Learning of Robust Deep Graph Matching: An Embedding Based Approach," *IEEE Transactions on Pattern Analysis and Machine Intelligence*, vol. 45, no. 6, pp. 6984–7000, 2023. DOI: 10.1109/TPAMI.2020.3005590.

[41] B. Jiang *et al.*, "GLMNet: Graph learning-matching convolutional networks for feature matching," *Pattern Recognition*, vol. 121, 2022. DOI: 10.1016/j.patcog.2021.108167.

[42] R. Wang *et al.*, "Unsupervised Learning of Graph Matching With Mixture of Modes via Discrepancy Minimization," *IEEE Transactions on Pattern Analysis and Machine Intelligence*, vol. 45, no. 8, pp. 10 500–10 518, 2023. DOI: 10.1109/TPAMI.2023.3257830.

APPENDIX A
SUPPORTING FIGURES

Fig. 12. MinIP segmentations generated from the classic UNet model [8]. (A)-(B) depict the anterior–posterior (AP) and Lateral views respectively.

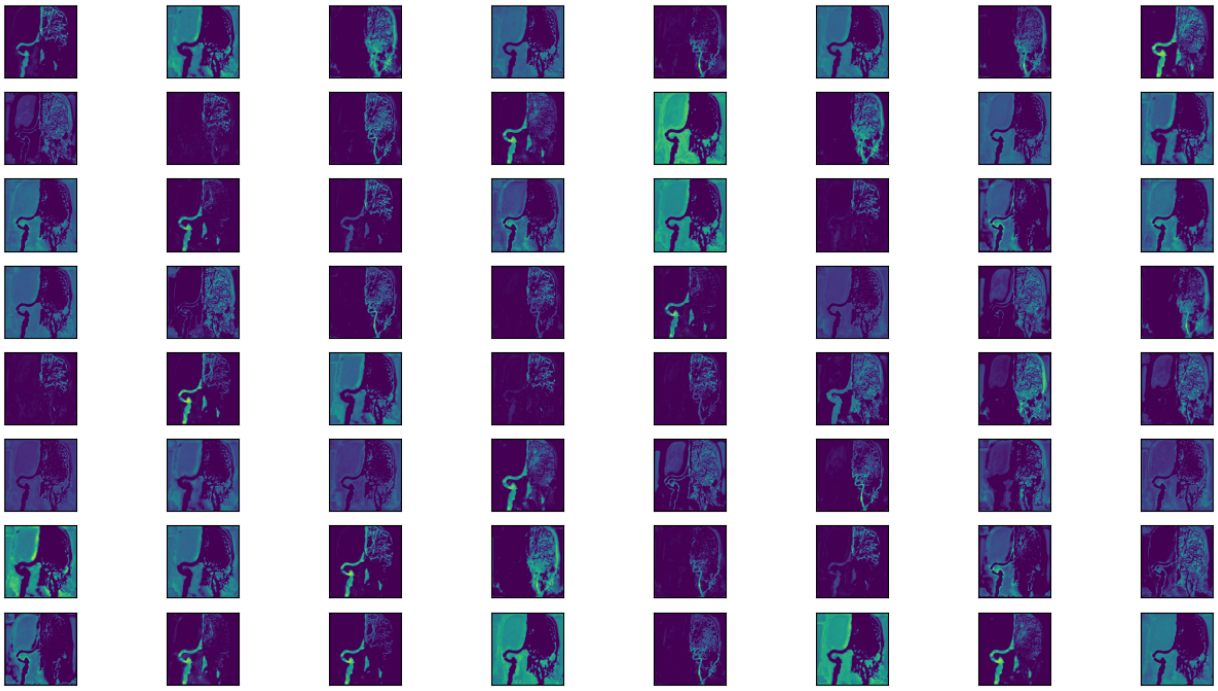

Fig. 13. 64 Extracted feature maps from the final layer of the Temporal UNet model [8].

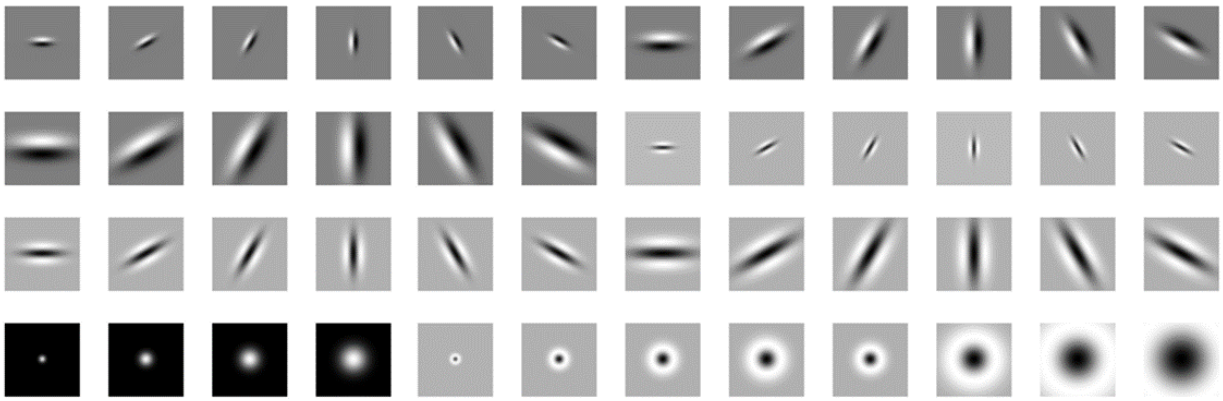

Fig. 14. 48 filters generated by the Leung-Malik Filter Bank. Starting from the top left moving right, the first 36 filters are the first and second derivatives of Gaussian filters, the next 4 are the Gaussian filters and the remaining 8 are the Laplacian of Gaussian filters, all with their respective orientations and scales.

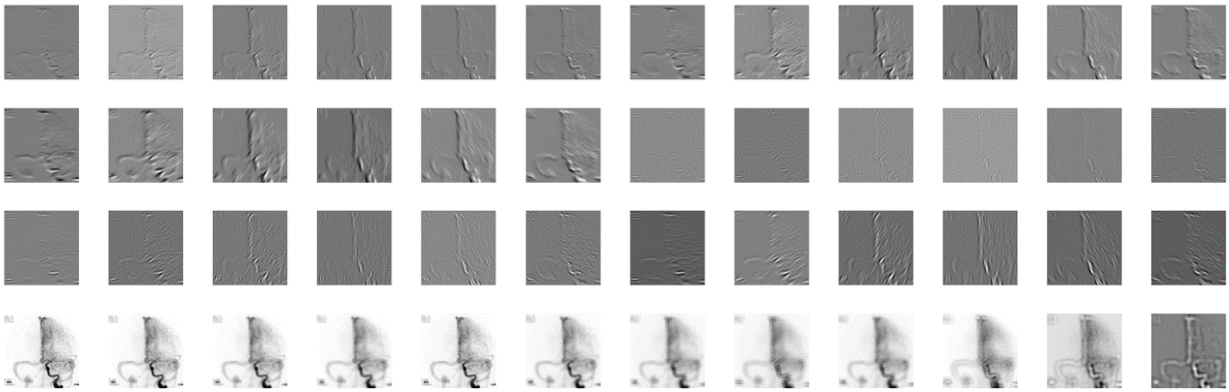

Fig. 15. 48 Extracted feature maps using the Leung-Malik Filters. The individual images match the individual filters provided in Figure 14.

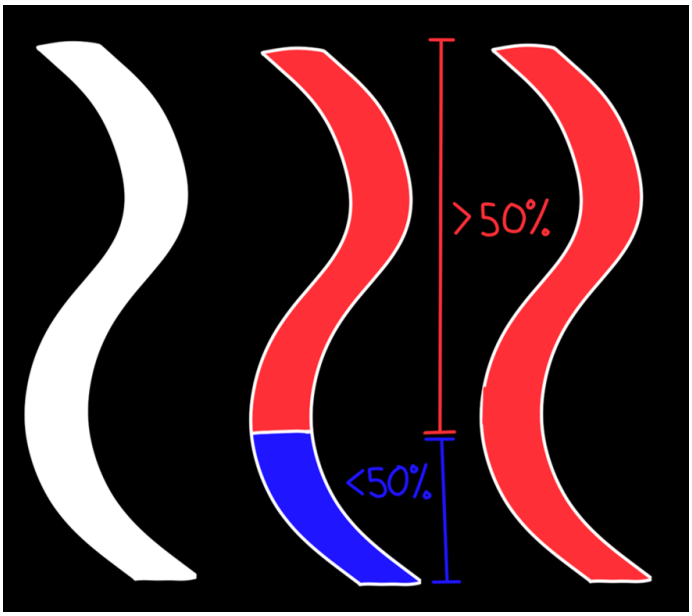

Fig. 16. Illustration of calculating matching segment using RB-VM. The left segment represents the segmentation of the original vessel segment being tested. The red and blue sections depict the matched and non-matched segmented pixels respectively. The right vessel segment depicts a matched vessel segment given that the number of matched segmented pixels exceeds the non-matched ones.

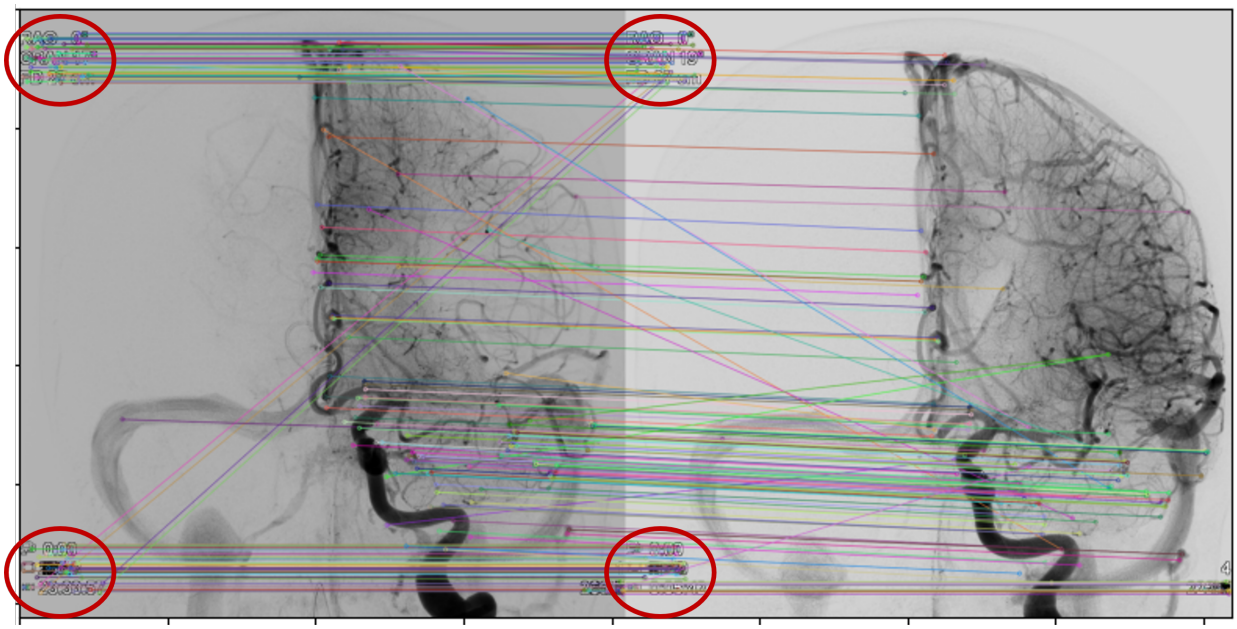

Fig. 17. Keypoint pairs detected via the SIFT algorithm on the MinIP pre-post images before the removal of unwanted text and borders. The circles point to multiple occurrences of text being matched. This prevented the calculation of a good transformation matrix and therefore a good registration.

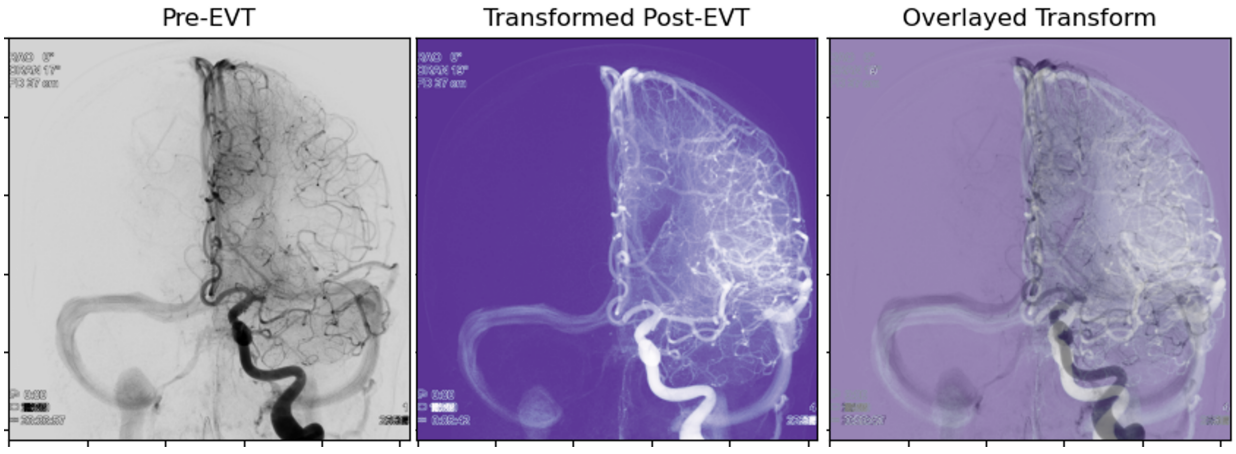

Fig. 18. SIFT transformation before the removal of unwanted text and borders from MinIP images.

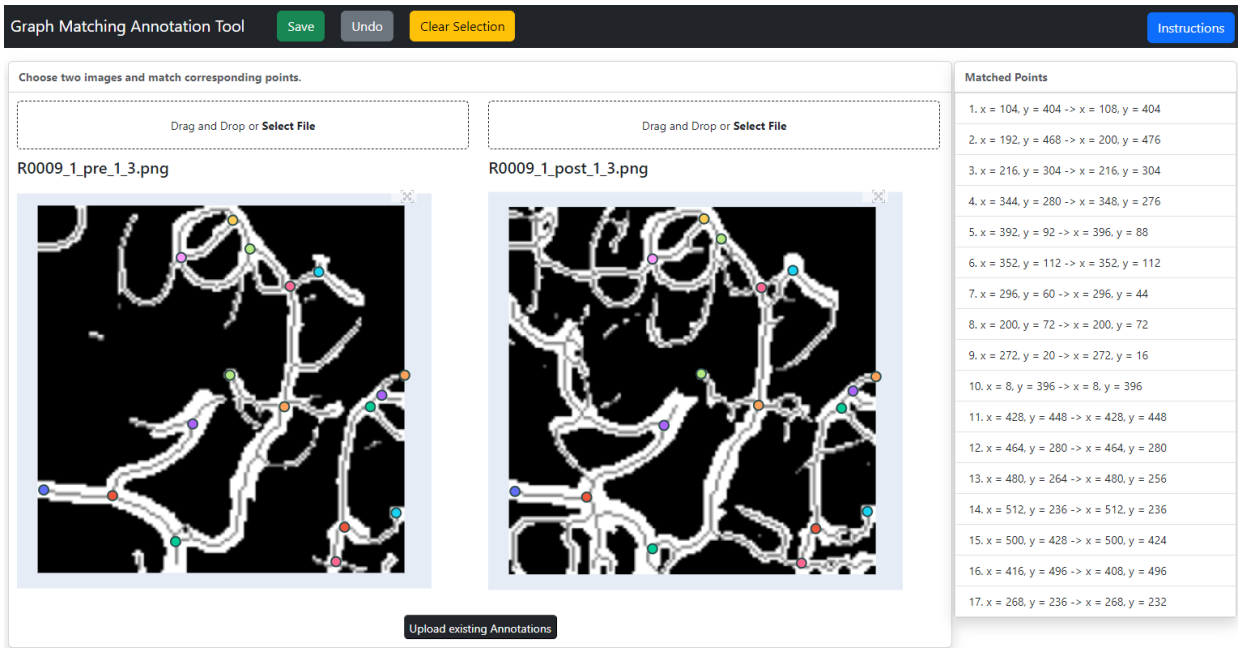

Fig. 19. Graph Matching Annotation Tool Interface used for generating the required annotations for quantitative evaluation of the proposed methods.

APPENDIX B
ADDITIONAL RESULTS

The additional comparisons present in this section provide insight in the different GB-VM methods performance as well as alternative permutations of parameters and their influence on each other. The recall metric is calculated using the evaluation dataset. Table IV looks at the effect of feature normalization based on the features used. The optimal neighborhood parameters calculated in Table II are used for all additional experiments.

TABLE IV
Experiments comparing the effect of feature normalization based on the features used. Bold values indicate the best performing parameter per experiment and underlined values indicate the best performing method.

Parameters		**Recall (%)**		
Features Used	Feature Normalization	GB-VM Patched (GB-VM-P)	GB-VM Single-Scale (GB-VM-SS)	GB-VM Multi-Scale (GB-VM-MS)
LM Features	None	**47.4**	**42.3**	**45.6**
	Z-score Standardization (Instance)	47.1	41.4	45.3
	Min-Max Normalization (Instance)	43.1	35.2	34.9
	Z-score Standardization (Distribution)	46.1	40.0	43.3
	Min-Max Normalization (Distribution)	39.6	29.4	30.3
LM Features + Coordinates	None	**51.5**	43.3	40.3
	Z-score Standardization (Instance)	50.4	**47.7**	**49.5**
	Min-Max Normalization (Instance)	47.3	43.6	41.3
	Z-score Standardization (Distribution)	46.9	46.2	49.4
	Min-Max Normalization (Distribution)	42.1	41.4	40.3
LM Features + Radius	None	**47.3**	42.3	45.3
	Z-score Standardization (Instance)	47.3	42.9	**45.9**
	Min-Max Normalization (Instance)	43.9	35.5	35.5
	Z-score Standardization (Distribution)	46.0	**43.8**	45.3
	Min-Max Normalization (Distribution)	40.1	30.1	30.2
LM Features + Coordinates + Radius	None	**51.5**	43.4	40.6
	Z-score Standardization (Instance)	51.2	**47.9**	48.7
	Min-Max Normalization (Instance)	48.5	44.7	43.1
	Z-score Standardization (Distribution)	47.2	45.9	**49.1**
	Min-Max Normalization (Distribution)	43.0	41.6	40.4

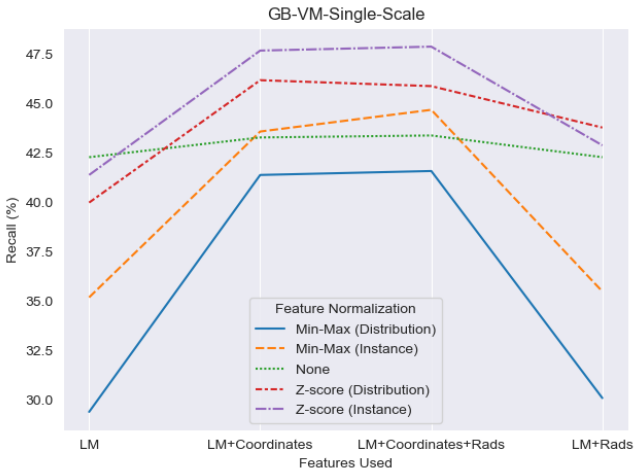

(a) GB-VM-Single-Scale (SS)

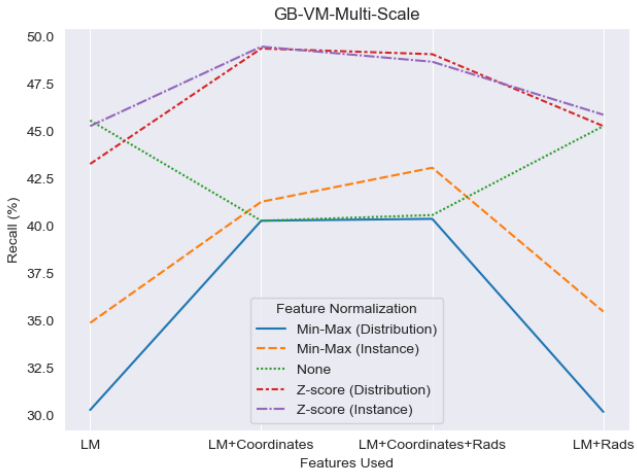

(b) GB-VM-Multi-Scale (MS)

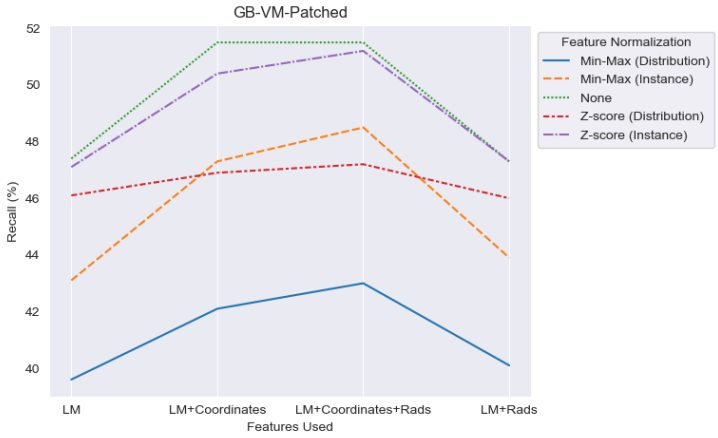

(c) GB-VM-Patched (P)

Fig. 20. Performance metric (Recall) line plots depicting the interaction of features used and type of normalization. The graphs are generated from the experiments presented in Table IV.

Table V, reports on the results when coordinates are always normalized between 0-1 using min-max normalization. Minimum and maximum values were decided based on the image shape. The normalization was performed to bring all feature values to similar scales and prevent specific features from having an increased effect. The coordinates had a uniform distribution based on the image shape. Therefore, min-max normalization was considered a good fit. The recall metric is calculated using the evaluation dataset.

TABLE V

Experiments comparing the effect of feature normalization based on the features used. The coordinates are always normalized using min-max normalization. Bold values indicate the best performing parameter combination per depending on the features used and underlined values indicate the best performing method.

Parameters		**Recall (%)**		
Features Used	Feature Normalization	GB-VM Patched (GB-VM-P)	GB-VM Single-Scale (GB-VM-SS)	GB-VM Multi-Scale (GB-VM-MS)
LM Features	None	**47.4**	**42.3**	**45.6**
	Z-score Standardization (Instance)	47.1	41.4	45.3
	Min-Max Normalization (Instance)	43.1	35.2	34.9
	Z-score Standardization (Distribution)	46.1	40.0	43.3
	Min-Max Normalization (Distribution)	39.6	29.4	30.3
LM Features + Coordinates	None	**47.4**	42.3	**45.6**
	Z-score Standardization (Instance)	47.2	42.6	45.4
	Min-Max Normalization (Instance)	47.3	43.6	41.3
	Z-score Standardization (Distribution)	46.2	**45.1**	43.5
	Min-Max Normalization (Distribution)	47.1	41.6	40.4
LM Features + Radius	None	**47.3**	42.3	45.3
	Z-score Standardization (Instance)	47.3	42.9	**45.9**
	Min-Max Normalization (Instance)	43.9	35.5	35.5
	Z-score Standardization (Distribution)	46.0	**43.8**	45.3
	Min-Max Normalization (Distribution)	40.1	30.1	30.2
LM Features + Coordinates + Radius	None	47.3	42.3	45.3
	Z-score Standardization (Instance)	48.2	42.9	**46.1**
	Min-Max Normalization (Instance)	**48.5**	44.7	43.1
	Z-score Standardization (Distribution)	46.2	**45.2**	45.6
	Min-Max Normalization (Distribution)	47.6	41.6	40.4

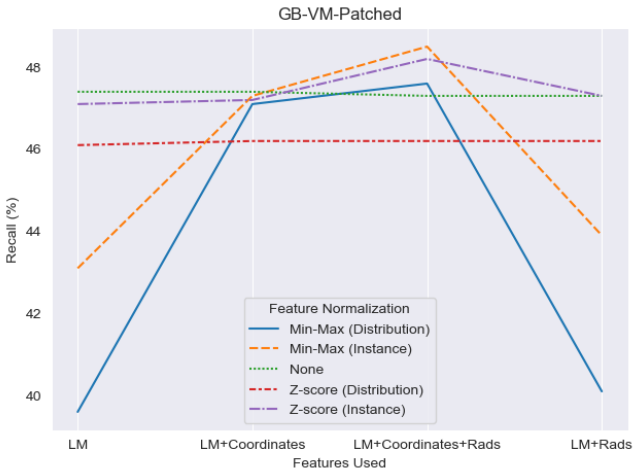

(a) GB-VM-Patched (P)

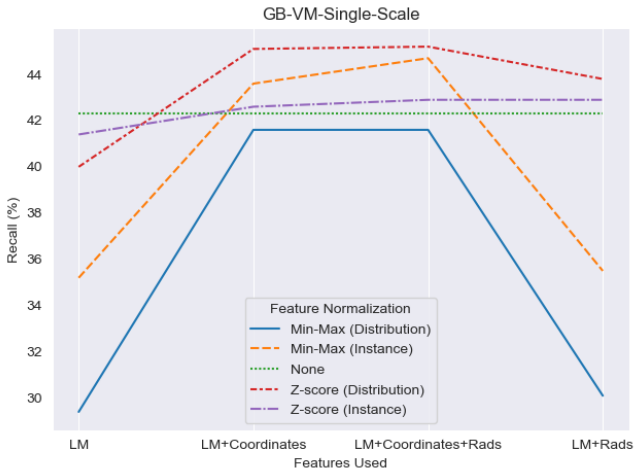

(b) GB-VM-Single-Scale (SS)

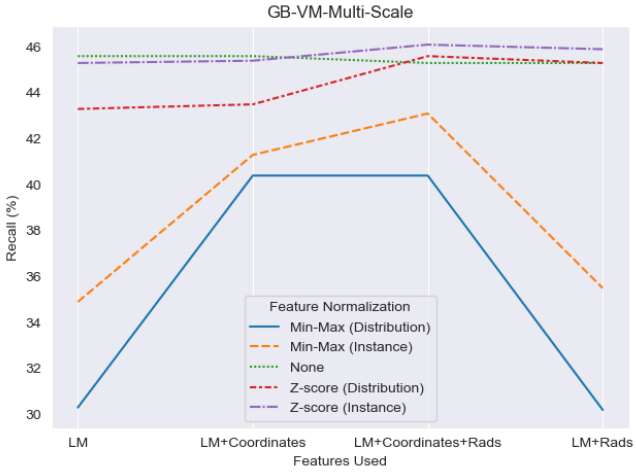

(c) GB-VM-Multi-Scale (MS)

Fig. 21. Performance metric (Recall) line plots depicting the interaction of features used and type of normalization. The graphs are generated from the experiments presented in Table V.

APPENDIX C
LITERATURE REVIEW

Graph Matching: A Short Survey of Recent Developments in Medical Imaging

Michael Angelo Berrospi

August 9, 2024

***Abstract*—This review explores the utilization of graph matching (GM) methodologies in the realm of medical imaging, outlining the foundational concepts, methodological classifications, variant implementations, and potential future trajectories. GM refers to the problem of finding node correspondence between graphs through maximizing node and edge similarities. The survey encompasses diverse inexact GM approaches, categorizing them into discrete methods, relaxation and replacement techniques, deep learning methodologies, and miscellaneous strategies. Discrete methods, such as tree search algorithms and Monte Carlo approaches, are computationally intensive yet proficient in certain medical imaging tasks. Conversely, relaxation techniques, including spectral and continuous relaxations, offer computational efficiency but may lack robustness. Deep learning methods, particularly Graph Neural Networks (GNNs), exhibit promise in enhancing GM efficacy, although their application in medical imaging is in its infancy. The review underlines the integral role of GM in medical imaging, leveraging graph representations of anatomical structures for diagnosis, procedural enhancement and post-procedural evaluation. Anticipating the evolution of GM with the integration of deep learning techniques, the review envisions improved performance and expanded applicability in medical imaging domains.**

***Index Terms*—Graph matching, correspondence, medical imaging.**

I. INTRODUCTION

GRaph matching (GM) is a classic and long studied computational problem that aims to find an optimal correspondence (matching) between vertices in two or more graphs. This can be achieved by maximizing their respective node and edge affinities. This problem has been studied extensively over the years for several reasons. Firstly, it has applications in many different fields and areas including but not limited to, pattern recognition, computer vision, bio-informatics and social networks [1, 2, 3]. Graph structures can naturally represent a multitude of real world data such as chemical compositions, transportation networks, social networks and medical structures such as brain connectomes and vessels. Medical imaging is a field that can benefit substantially from the graphical representation of structures and use of graph matching. This applies especially in situations where a comparison of data acquired at different time-points can provide important insights, helping with diagnosis or procedure follow-up. An example to illustrate such a case is the scenario where an informative intra-patient follow-up of liver tumors can be achieved by applying vascular matching [4]. Moreover, GM has had continuous ongoing research due to its vast range of applications. It has an NP-hard nature, as it can generally be formulated as a quadratic assignment problem (QAP), which is considered one of the hardest combinatorial optimization problems in existence [1, 2, 5, 6].

This survey does not aim to provide a complete overview of graph matching techniques. Instead, it aims to complement the vast pool of surveys on this subject, focusing on recently developed techniques, and more specifically, ones related to medical imaging. We focus on this field as the surveys combining graph matching techniques and medical imaging are scarce and in need of further exploration. For more extensive information on graph matching techniques the reader is referred to [1, 3, 7, 8, 9, 10, 11]. In this work, we intend to give an overview of the main GM methodologies encountered in the field of medical imaging and briefly explain a number of different approaches.

The GM problem can be classified in two well defined families as defined by many other works: exact and inexact matching. The first one is based on finding a strict correspondence or in other words a bijection of two graphs. For this bijection to be possible, the two graphs must have the same number of vertices. On the other hand, inexact matching accounts for differences between the graphs and the problem is relaxed, allowing an error-tolerant solution. The latter approach aligns best with real-world problems, since a matching between dissimilar graphs is usually addressed [1]. This can easily be demonstrated when considering the dissimilarities in medical imaging, which can be caused by different imaging modalities or conditions and/or interventions [3]. For instance, consider the case of vascular imaging pre and post an endovascular thrombectomy (EVT) intervention. The number of vertices, traditionally defined as vessel bifurcation and endpoints, as well as the structure of the two graphs will clearly differ. In detail, vessels following an occlusion are not visible in pre-EVT imaging but are visible in post-EVT imaging, if the procedure is successful. Due to these inherent differences in structure,topology and node count present in scenarios where graphs are extracted and utilized in medical imaging applications, this papers focus is on inexact graph matching techniques and directs the reader to [11, 12] for more information on exact graph matching.

The databases used for this study were Google Scholar and PubMed using a series of search strings. Namely, the following have been used in both databases, in unison or in several combinations, (graph matching) AND (medical imaging), (deep graph matching) AND (medical imaging), (intra-patient) AND (matching), (graph matching[Title/Abstract]) AND (medical imaging), (correspondence) AND (medical imaging), (Graph neural network) AND (graph matching), (Unsupervised graph matching). Furthermore, seed platforms like Litmaps, Con-

nected Papers and Research Rabbit were utilized together with collected literature to discover additional related works that were not captured by the search terms.

This work is structured as follows. Section II provides insight on the fundamentals of graph matching including the basic formulations and definitions. Section III contains a semi-complete overview of main methodologies encountered over the years and more recent developments. This section also includes how these approaches were employed in medical imaging. Lastly, Section IV and Section V conclude this work by discussing the findings and possible future developments.

II. Fundamentals of Graph Matching

A. Problem Definition

A graph of size n (i.e., numbers of nodes) can be represented as $G = (\mathcal{V}, \mathcal{E}, A, X, E)$, in which $\mathcal{V} = v_1, \cdots, v_n$ denotes the set of nodes (also known as vertices), $\mathcal{E} \subseteq \mathcal{V} \times \mathcal{V}$ denotes the set of edges, $A \in \{0,1\}^{n \times n}$ denotes the adjacency matrix, $X \in \mathbb{R}^{n \times d}$ denotes the initial feature matrix of nodes, and $E \in \mathbb{R}^{n \times n \times d}$ denotes an optional initial feature matrix of edges, as described in [13]. A feature matrix can be expressed as a row-wise concatenation of feature vectors where the number of rows is defined by the number of nodes (or edges) and the number of columns is devised from the number of features [13]. Different variations of this representation can be found in literature.

The aim of the graph matching problem is to identify the optimal node-to-node correspondence between two input graphs, specifically G_1 and G_2. Generally, the two-graph matching problem can be expressed by Lawler's QAP form:

$$\begin{aligned} &J(S) = \text{vec}(S)^T K \text{vec}(S) \\ &\text{s.t} \quad S^T 1_{n_1} \leq 1_{n_2}, \quad S 1_{n_2} = 1_{n_1} \end{aligned} \tag{1}$$

where $\text{vec}(S)$ represents the vectorized version of the assignment matrix $S \in \{0,1\}^{n_1 \times n_2}$ (also known as correspondence or permutation matrix) between two graphs, i.e $S_{ij} = 1$ means that node $v_i \in G_1$ corresponds to $v_j \in G_2$ and otherwise $S_{ij} = 0$, $K \in \mathbb{R}^{(n_1 \times n_2)^2}$ is the second-order affinity matrix where each element $K_{ij,ab}$ indicates the level of correspondence between nodes $(v_i, v_j) \in G_1$ and $(v_a, v_b) \in G_2$. Specifically, the diagonal and off-diagonal elements represent the node-to-node and edge-to-edge similarity respectively, as described by [14, 13]. Lastly, 1_n is a column vector of length n whose elements are equal to 1 and the constraints enforce a one-to-one assignment between nodes and a $\mathcal{V}_1 \leq \mathcal{V}_2$ node count. The aim is to find the optimal assignment matrix S that maximizes the affinity score $J(S)$ [1, 8]. This formulation has been widely adopted in literature [1, 13, 5, 8].

Additionally, another QAP form for two-graph matching is known as the Koopmans-Beckmann's QAP and can be described by:

$$J(S) = \text{tr}(S^T A_i S A_j) + \text{tr}(K_p^T S) \tag{2}$$

where A_i and A_j are the weighted adjacency matrices of graph G_1 and G_2 and K_p is the node affinity matrix. It should be noted that, this formulation can be regarded as a special case of Lawler's QAP by setting $K = A_j \otimes A_i$, where $\otimes$ signifies the Kronecker product operation [1, 14, 8]. We also offer an example illustration of the node-to-node correspondence in a real life scenario related to medical imaging in Figure 1.

B. Additional Formulations

1) ***Factorized Affinity Matrix.*** Zhou and De la Torre [14] presented a way to factorize the affinity matrix as:

$$K = \text{diag}(\text{vec}(K_p)) + (G_2 \otimes G_1)\text{diag}(\text{vec}(K_q))(H_2 \otimes H_1)^T \tag{3}$$

where $G, H \in \{0,1\}^{n \times m}$ are incidence matrices, i.e $G_{i_c} = G_{j_c} = 1$ if the c^{th} edge starts from the i^{th} node and ends at the j^{th} node; $K_p \in \mathbb{R}^{n_1 \times n_2}$ indicates the node affinity matrix, with n number of nodes, and $K_q \in \mathbb{R}^{m_1 \times m_2}$ indicates the edge affinity matrix, with m number of edges. The diag(k) represents a diagonal matrix whose diagonal elements are k. The formulation includes two incidence matrices as it represents the general case that can handle both directed and undirected graphs. Additional information on this factorization can be found in the original work.

2) ***Higher-Order Graph Matching.*** So far the previous formulations only consider the affinity between vertex and edges, also known as first-order and second-order respectively. An alternate formulation used considers higher-order affinity as it compares the differences between super or hyperedges [1, 9]. Hyperedges are composed of 3 or more nodes and could likely produce a more robust correspondence. The formulation takes a tensor format as:

$$\begin{aligned} &J(s) = H \otimes_1 s \otimes_2 s \cdots \otimes_m s \\ &\text{s.t} \quad S^T 1_{n_1} \leq 1_{n_2}, \quad S 1_{n_2} = 1_{n_1} \end{aligned} \tag{4}$$

where s=vec$(S) \in \{0,1\}^{n_1 \times n_2}$, m is the order of the affinity tensor and H is the affinity tensor.

III. Methodologies

In line with previous works regarding GM [3, 12, 8, 9, 15], we arrange the different inexact matching methodologies in categories as presented in Figure 2; Discrete methods, Relaxation and Replacement, Deep Learning methods and Miscellaneous.

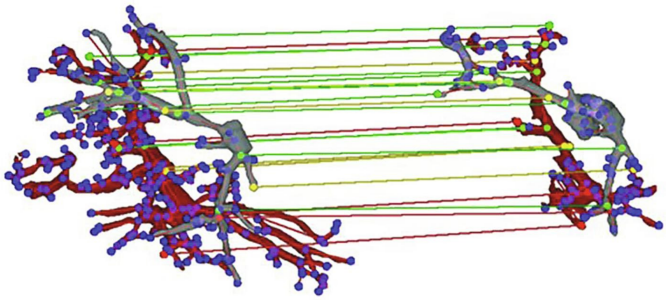

Fig. 1. The structure on the left shows the liver vasculature before a tumor resection, while the structure on the right displays the vasculature after the procedure. The vascular tree is depicted as a graph, where bifurcations serve as anatomical landmarks indicated by blue spheres (vertices). A graph matching method was used to detect correspondences between the vascular trees as shown by the green and red lines connecting the structures [3].

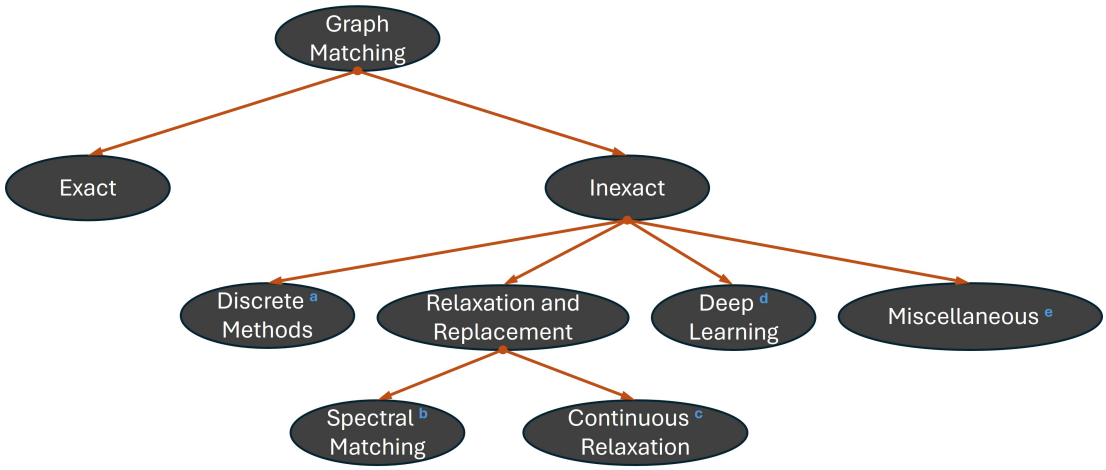

Fig. 2. Proposed graph matching methods categorization

a. Charnoz et al. [4], Zhu et al. [16], Pinheiro et al. [17], Zhu et al. [18], Lajevardi et al. [19], Shen et al. [20], Olivera et al. [21], Osmanlioglu et al. [22, 23], Olafson et al. [24], Bukhari et al. [25], Serradell et al. [26, 27], Garcia Guevara et al. [28, 29], Czajkowska et al. [30], Bai et al. [31].

b. Umeyama et al. [32], Smeets et al. [33], Im et al. [34], Guo et al. [35], Lombaert et al. [36], Shakeri et al. [37, 38], Wright et al. [39], Leng et al. [40], Chen et al. [41, 42], Zhou et al. [43].

c. Groher et al. [44], Almasi et al. [45], Deng et al. [46], Metzen et al. [47, 48], Liu et al. [49, 50, 51], Zaslavskiy et al. [52], Calissano et al. [53], Wang et al. [54].

d. Zhao et al. [55, 56, 57], Furukawa et al. [58, 59], Mikamo et al. [60, 61].

e. Moriconi et al. [62], Guo et al. [63], Motta et al. [64], Zhu et al. [65], Riffaud et al. [66], Rist et al. [67], Behkamal et al. [68], Yao et al. [69], Rochman et al. [70], Buskulic et al. [71], Yadav et al. [72, 73].

A. *Discrete Methods*

Discrete methods attempt to solve the GM problem in the discrete domain. Categories of algorithms that fit this paradigm include but are not limited to, Tree Search, Integer Projected Fixed Point (IPFP), Monte Carlo approaches, Branch and Bound and Graph Edit Distance (GED). A number of these methods have been applied to medical imaging and are presented here.

Perhaps one of the first attempts to GM using medical imaging was performed by Charnoz et al. [4]. They proposed a tree matching algorithm to match liver vascular systems between two CT acquisitions with the goal of making an intra-patient follow-up of tumors. In more detail, they model the liver vasculature as a tree with nodes and edges representing bifurcations and vessel connections respectively. Then, they follow an iterative approach where, starting from the tree roots, they focus on the most probable solutions consisting of a set of matches, examine the probable solutions at each tree depth step and update the solution. The probable solutions are evaluated by quality match criteria consisting of several cost functions, to limit the selection of possible tree matching solutions. In a similar fashion, Zhu et al. [16] present a heuristic tree searching technique for 3D/2D rigid registration of vessel structures. Their approach comprises of GM and registration phases. The vessels are represented as a graph where vertices represent bifurcations and endpoints and edges represent the connections. They propose that a matching of graphs can be represented as vertex and edge pairs and follow a successive tree search procedure using either an evolution of the A* search algorithm or a greedy tree search based on best-first search. This procedure is divided into states whose combination constructs the complete search tree. Each state is characterized by adding a new superedge pair, controlled by a set of conditions, and updating the vertex and edge pairings.

Monte Carlo tree search is another technique that has been used successfully for the GM problem within the medical imaging domain. Pinheiro et al. [17] recently used said technique to register vessels in retinal fundus images, brain circuit scans and heart angiograms and neurons in brain circuits. In addition, they make use of hyperedges to increase the robustness of their results. Additionally, they establish a set of rules and a transformation model to guarantee the feasibility of newly added matches to the final set. The approach is capable of processing extensive graphs in a prompt and effective manner. A similar technique was used by Zhu et al. [18] for 3D CTA to 2D DSA vessel registration and was tested on the hepatic and coronary arteries and the aorta.

In many cases, Munkres's algorithm (also known as the Hungarian Method) has been used to find correspondences between graphs. The Hungarian Method results in a discrete assignment matrix calculated based on the minimization of a cost matrix. Lajevardi et al. [19] proposed an automatic retina verification framework based on GM applied on the retinal vasculature. The GM step utilizes a modified Hungarian method, with the cost matrix representing the cost of edit operations to convert G_1 to G_2. Their methodology outputs the minimum graph edit distance between the two graphs and the graph edit path indicating the optimal set of edit operations

TABLE I
CLASSIFICATION ACCORDING TO IMAGING MODALITY

Glossary: CT: Computed Tomography, CTA: Computed Tomography Angiography, CBCT: Cone-Beam CT, MRI: Magnetic Resonance Imaging, MRA: Magnetic Resonance Angiography, DSA: Digital Subtraction Angiography, EM: Electron Microscopy, LM: Light Microscopy, C-EM: Cryo-Electron Microscopy, AOSLO: Adaptive Optics Scanning Light Opthalmoscopy.	
CT (including CTA,CBCT):	Charnoz et al. [4], Zhu et al. [16],Zhu et al. [18], Garcia Guevara et al. [28, 29], Czajkowska et al. [30], Smeets et al. [33], Groher et al. [44], Metzen et al. [47, 48], Zhu et al. [65], Riffaud et al. [66], Rist et al. [67], Yao et al. [69], Rochman et al. [70]
MRI (including f-MRI,MRA,T1-MRI,Diffusion MRI):	Shen et al. [20], Osmanlioglu et al. [22, 23], Olafson et al. [24], Bukhari et al. [25], Im et al. [34], Lombaert et al. [36], Shakeri et al. [37, 38], Wright et al. [39], Leng et al. [40], Chen et al. [41, 42], Groher et al. [44], Almasi et al. [45], Metzen et al. [47, 48], Calissano et al. [53], Moriconi et al. [62], Guo et al. [63], Buskulic et al. [71]
X-ray (including DSA, X-ray Angiography):	Zhu et al. [16], Pinheiro et al. [17], Zhu et al. [18], Serradell et al. [26, 27], Guo et al. [35], Groher et al. [44], Zhao et al. [55, 56, 57], Zhu et al. [65]
Microscopy (including EM, LM, C-EM):	Pinheiro et al. [17],Serradell et al. [26, 27], Behkamal et al. [68]
Retinal Fundus Imaging or AOSLO:	Lajevardi et al. [19],Serradell et al. [26, 27], Deng et al. [46], Liu et al. [49, 50, 51], Motta et al. [64]
Infrared Breast Imaging:	Olivera et al. [21]
Endoscopy	Wang et al. [54], Furukawa et al. [58, 59], Mikamo et al. [60, 61]
3D Rotational Angiography	Almasi et al. [45]
Structured light 3D body scanner	Zhou et al. [43]

to convert one graph to the other. These are then used to create a maximum common subgraph. Moreover, Shen et al. [20] proposed a GM based method to quantify connectomic similarity then used it to provide a subject-specific score allowing them to separate patients and controls in traumatic brain injury cases. Specifically, they use GED and define the cost matrix of operations (insertion, deletion, substitution) as the Manhattan distance weighted by a coefficient learned through Markov chain Monte Carlo. The correspondence between nodes can be extracted from the edit path if that path matches a node to its counterpart. However, the problem is intractable and they calculate an approximate solution using the Hungarian method. A similar approach was followed by Olivera et al. [21]. Their method finds graph correspondences using an adaptation of the graph edit distance as presented by Armiti and Gertz [74]. They iteratively compute the edit distance based on vertex operations costs, similar to GED, calculate the minimum distance matrix and finally use the Hungarian method to obtain a final correspondence matrix. Differing from the previous works in terms of the use of GED, Osmanlioglu et al. [22] proposed a matching accuracy acquired through GM as an affinity metric to compute the resemblance between structural and functional connectivity in the brain. Their method also employed the Hungarian method with the cost matrix comprised of the Euclidean distance between node feature vectors. They applied their method on functional and structural connectomes created after imaging using functional and diffusion weighted Magnetic Resonance Imaging (MRI). The same authors used the matching accuracy as described in this work to investigate the consistency of functional connectomes in later work [23]. The connectivity of the brain was additionally explored by Olafson et al. [24] where GM was used to capture longitudinal Functional Connectivity (FC) reorganization in stroke patients. Closely resembling the work of [22], they used the Hungarian method to solve the assignment problem where the cost matrix comprised of the Euclidean distances between the partial correlation-based FC matrices of two regions. Functional connectome work was recently expanded by Bukhari et al. [25]. Following the previous works on FC differences between individuals, they proposed a GM approach aiming to develop an inter-individual functional connectome metric that measures the distance between individuals' partial functional connectivity matrices. They alter the method used by [22, 24] by adding an additional penalty or regularization term to the problem formulation and solve it using the Hungarian method in an iterative fashion until convergence of the objective function is reached. Consequently, the matching results are used to construct the targeted metrics.

Serradell et al. [26] introduced the idea of using Gaussian processes to find correspondences and tested said idea on angiography images of the heart, brain blood vessels and neuronal trees. They achieve elastic registration based on the graph matching method proposed. In more detail, their GM method consists of finding an initial set of node matches to instantiate the Gaussian Process (GP). The GP is then refined and finally a geometric mapping is obtained, where given a node, its match in the second graph is determined by its mean and covariance. The GP's goal is to predict the mapping of nodes in G_1 and minimize the set of potential matchings. The most likely prediction based on geometric and other criteria is chosen to refine the GP. This method includes two improvements from the original paper [27], the introduction of non-linear regression to the GP and the combination of active testing and bayesian models. Garcia Guevara et al. [28, 29] improved upon this method twice. First, they combine the method with biomechanical modelling which allows the model to handle large deformations. Additionally, they use an adaptation of the work by Seradell et al. [26], introducing the improved Gaussian process regression, by adding further constraints during the matching procedure when the hypothesis space is large. This resulted in less computational costs. Their

method was applied on the synthetic data of the liver portal vein tree and porcine liver data acquired using Computed Tomography (CT) and Cone Beam CT (CBCT). Their method was later further enhanced, as it used a new biomechanical vascularized liver model, allowing it to find correspondence via a compliance-based adaptive search. This approach was tested on vascular graphs segmented from Computed Tomography Angiography (CTA) and a porcine liver dataset acquired by CTA.

In the work of Czajkowska et al. [30] two methods for 3D registration of pre-post operation CTA in abdominal aortic aneurysm cases are explored. One of the methods is known as skeleton GM as proposed by Bai et al. [31]. The method finds correspondence between two graphs by establishing a matching of their end nodes only using skeleton graphs. The correspondence is determined by computing a dissimilarity cost matrix and using the Hungarian method to reach the final discrete assignment matrix.

B. Relaxation and Replacement

Relaxation is a common way to approach the GM problem as given the original formulation the problem is intractable and has an NP-hard nature. Common relaxation approaches include spectral, continuous, convex, and convex-to-concave relaxation. Due to the overlap of relaxations in different approaches which leads to vague classifications, we divide this section in spectral and continuous relaxation methods. Spectral relaxations conventionally transform the GM problem to an eigenvector problem which can then be solved by a number of strategies [75]. Continuous relaxations commonly relax the original problem from discrete to continuous space and follow a discretization procedure afterwards to return back. Given their similarity to convex and convex-to-concave relaxations, all of them are grouped under this category. A multitude of relaxation techniques have been used and applied in medical imaging and a number of them are presented in this section.

1) ***Spectral Matching.*** Spectral matching was originally proposed by Umeyama et al. [32], where the idea revolved around performing eigendecomposition on the adjacency matrices of both graphs, attaining the absolute values of the eigenvector matrices and employing the Hungarian method to obtain the assignment matrix. This method later inspired a number of different approaches.

The majority of work has been inspired by methods used in alternate fields. For instance, the work of Scott and Longuet-Higgins [76] was used by Smeets et al. [33] to find a matching between 3D lung vessel trees. Briefly, the spectral technique performs singular value decomposition on a previously created soft correspondence matrix constructed using bifurcation matching probability measures. Moreover, the correspondence technique by Leordeanu and Hebert [77], a common method used in computer vision, was employed by Im et al. [34] to find correspondences between sulcal graphs. In their approach, they computed a similarity matrix based on the feature affinity of nodes. The permutation matrix was then calculated using Leordeanu and Heberts' [77] technique. Furthermore, Guo et al. [35] used an altered version of the method called Spectral Matching with Affine Constraints (SMAC), initially proposed by Cour et al. [78] in order to identify landmark correspondence in hand X-ray images. In the original method the similarity between possible matches is calculated by their geometric distance and angle and an energy function is defined, in order to maximize a quadratic score function, which is then solved by a spectral relaxation technique. Guo et al. [35] improve this approach by refining the construction of the affinity matrix and adding sparsity on the assignment matrix to exclude ambiguous matches. Then they reformulate the energy function and solve it using a region reflective algorithm followed by the Hungarian method. Lastly, this approach is integrated in an iterative hierarchical matching framework consisting of the proposed sparse GM and thin-plate spline based interpolation.

Lombaert et al. [36] approach the spectral matching technique in a slightly different way. Their work presents a surface matching method. While it is does not solve a strictly GM problem it is included due to its similarity. The method is applied to brain surface matching. Specifically, their algorithm uses eigenvalues and eigenvectors produced through eigendecomposition of the Laplacian matrices of graphs to produce node correspondences and is used for feature matching as a special kind of regularization. Shakeri et al. [37] proposed a slightly altered method inspired by Lombaert et al. [36] used to identify regional morphological differences in subcortical structure between healthy subjects and subjects with Alzheimer's disease. They improve the method by adding a final smooth mapping by introducing an association graph using the initial correspondence map between the surfaces, and performing a similar Laplacian eigendecomposition matching step. The same authors use the original approach as a primary step for Alzheimer's disease classification [38]. Wright et al. [39] obtain a cortical surface correspondence in data collected from in utero MRI of fetuses. Their method is an extension of the one proposed by Lombaert et al. [36]. Following [36], they obtain a correspondence map based on the shortest Euclidean distance in the spectral domain. Their adaptation includes the use of additional surface descriptors (mean curvature and surface normal direction) and edge-based smoothing as a form of regularization. Additionally, Leng et al. [40] applied a similar method for image matching using brain images obtained through MRI. In more detail, they use a normalized version of the Laplacian matrices followed by singular value decomposition. The resulting eigenvectors are used to compute an affinity matrix from which the final matching is extracted.

Unlike the approaches explored so far where determining some form of correspondence was the goal, Chen et al. [41] perform a GM technique to reduce noise occurring in diffusion MRI images. Concisely, they perform neighborhood matching based on features derived from a graph Laplacian decomposition. Additionally, in their later work [42], they propose additional improvements to this algorithm, one of which is the introduction of Gaussian kernels when defining the affinity weight between node pairs.

Lastly, the following technique followed a spectral approach

which is not strictly a spectral matching method but is fairly similar and is therefore included. Zhou et al. [43] integrated the spectral matching by [36] followed by coherent point drifting, a well known point matching approach, for the purpose of 3D human shape landmark detection.

*2) **Continuous Relaxation.*** One of the first works targeting GM in the continuous realm was proposed by Gold and Rangarajan [79] and is well known as Graduated Assignment (GA). They formulate the GM problem as defining an assignment matrix while taking into account a compatibility matrix that denotes the link compatibility between two graphs. Their final formulation includes a continuous assignment matrix (also known as a softassign) made possible by the Sinkhorn method. This allowed them to develop an assignment problem which was solved iteratively until convergence was reached using a deterministic annealing scheme. Groher et al. [44] incorporated this method in their approach for the task of 2D to 3D registration of vascular structures derived from angiographic scenes. Vascular registration was similarly explored by Almasi et al. [45] and was tested on cerebrovascular MRA and 3D rotational angiography (3DRA) images. Their method included node and edge attributes that incorporated geometrical information which allowed them to relax the problem to a linear assignment problem. This problem is then solved using an adapted version of the GA. Additionally, the same method by [79] was utilized as a principle step in registering retinal fundal vessel shape models using vascular structure graphs [46].

Metzen et al. [47, 48] followed the association graph approach proposed by Pelillo et al. [80, 81] to match liver and lung vascular trees. The method is not strictly a GM method as the problem is a continuous formulation of the maximum clique problem, however a matching is produced and we therefore decided to include it.

Moreover, Liu et al. [49] introduced a GM technique that utilizes the dual decomposition (also known as Langragian relaxation), which is known to be convex and continuous, to solve a model comprised of visual similarity and geometric constraints. Their purpose was to find correspondences between cone photoreceptor neurons. Their method is evaluated on a longitudinal adaptive optics scanning light opthalmoscopy dataset. The authors used the same technique in two other cases. First, they utilize it as a seminal step to identify paired patterns in longitudinal retinal pigment epithelium images[50]. Specifically, they use the GM technique to calculate affine invariant maximal stable extremal region matchings in Gaussian scale-space in order to approximate image displacement. Second, they apply GM for cell centroid correspondence consequently used for label transferring [51].

Furthermore, Zaslavskiy et al. [52] approached the GM problem using a reformulation to a least-square problem and convex-concave relaxations controlled by continuous parameters. The result was obtained through iteratively solving the Franke-Wolfe algorithm. In addition, they consider the assignment matrix as doubly-stochastic.

Calissano et al. [53] follow the GM algorithm propose by Vogelstein et al. [82] to align structural connectomes of healthy individuals, considering division of different granularity to gain knowledge on the connectivity misalignment between regions. The method in [82] relaxes the correspondence matrices from the discrete domain to the continuous using doubly stochastic matrices. The matching solution is calculated via gradient descent and it is noteworthy that a permutation matrix initialization is necessary.

A different approach is proposed by Wang et al. [54] where they solve the GM problem using a probabilistic way based on mean field theory in order to register 3D supine and prone colonography scans. In detail, the objective function resembled the Ising model with quadratic interaction. The expectation of the assignment matrix is approximated using mean field theory and resembles the confidence of a match. To maintain a one-to-one matching they solve the problem iteratively by maintaining the higher expectation at each step.

C. Deep Learning Methods

Deep learning and in general the field of machine learning have seen significant improvements in the past years. These techniques have been used in a multitude of fields to solve a vast number of problems. Computer vision is a field where deep learning models have been utilized extensively and their efficacy has been undoubtedly proven. Given the similarities, medical imaging is an area that is steadily migrating towards the use of such techniques. In the case of GM, recent developments in deep learning have introduced alternative ways to solve it. Most importantly, Graph Neural Networks (GNNs) are a type of neural network specifically designed to deal with graph representations. Recent works in domains outside of medical imaging have proven the usefulness of these networks when working with graph-like data. GNNs have been proposed as a way to solve the GM problem and have been successfully used in domains like computer vision and their effectiveness in solving the QAP is promising [83]. Their use in medical imaging applications is yet to be fully explored, but the following section provides some examples of how deep learning has been utilized to solve the GM problem in the field.

Zhao et al. [55, 56, 57] have presented three different approaches to solve the GM problem as a way to semantically label coronary arteries acquired from invasive coronary angiograms. It is important to note that all these networks operate in a supervised fashion where ground truth data is necessary. In their first approach [55], they defined an association graph that simulates the connectivity between to graphs. This allowed them to convert the problem to a vertex classification problem. They then developed a network where the three main components were a feature embedding and feature decoding module and a Graph Convolutional Network (GCN). Finally, the network was trained using cross entropy loss between the prediction and the ground truth. Their second approach [56] follows a similar structure with one clear change. The change is marked by the inclusion of an attention mechanism through using a Graph Attention Network (GAT). Their most recent method [57], enhanced their previous work with the goal of achieving real-time inference. Their enhancements include the use of hypergraphs (3-uniform), the addition of

node and edge attention via graph transformer networks and the use of uncertainty quantification via a true class probability approximation.

Focusing on a different application, Furukawa et al. [58] suggested a robust GM method with the purpose of auto-calibrating an active-stereo-based 3D endoscopic system. Their GM method was used to obtain correspondences between the graph represented original and detected pattern. Specifically, the correspondence estimation was achieved using a GCN approach applied to node feature vectors and the equivalent graph adjacency matrix of one graph and outputted a matching node ID on the second graph. This resembles a classification problem and was trained in a supervised fashion. The same authors developed the method further by using GCN on the node feature vectors of two graphs [60]. The matching was then attained using the cosine similarity of the produced feature embeddings and the model was trained again in a supervised fashion. Furukawa et al. [59] further used a very similar approach to [60] enhancing it through combining the achieved similarity matrix with epipolar constraints in the matching procedure. This is then used for auto-calibration and shape reconstruction and was evaluated on bio-tissues and a colon phantom. This method is then used once again for an identical purpose [61].

D. Miscellaneous

This section includes methods for which an accurate categorization could not be achieved or cases where the method used was not strictly a GM approach but served a similar purpose.

Zhou and De la Torre [14] presented a different formulation to the GM problem which was introduced in Section II, and introduced a factorized GM (FGM) approach based on it. Their method was employed by Moriconi et al. [62] along with other common techniques. Namely, they implemented GA, Spectral Matching, SMAC, Probabilistic Matching, IPFP and Re-weighted Random Walks in order to compare their performance in determining an elastic registration of vascular graphs. Importantly, they presented a novel formulation of the vessel structures as over-connected geodesic graphs and preceded the GM with a coarse geometrical alignment using the globally-optimal Iterative Closest Point (ICP) algorithm. Guo et al. [63] use the same FGM to match elastic shape graphs devised from brain arterial networks as part of developing a statistical analysis of said networks.

Motta et al. [64] proposed an alternate reformulation to the original GM problem. In more detail, they model the registration of vessels in retinal fundus images as a GM problem formulated as a discrete optimal transport (OT) problem. The OT cost function is specified using particular similarity measures, and this formulation relaxes the problem to a linear model solved using mixed integer linear programming.

Furthermore, Zhu et al. [65] targeted 3D to 2D coronary artery registration via an iterative closest GM procedure. Their framework included matching and transformation phases. The matching phase is based on redundant GM which in simple terms introduces redundant edges. These edges lead to a denser affinity matrix which increases the probability of correct matches. A fine vessel matching is then obtained based on the node correspondences.

Moreover, abdominal aortic identification is achieved using a kind of GM technique by Riffaud et al. [66]. Their approach does not strictly consider the GM problem but they attain a matching of the abdominal arterial system to trees extracted via segmentation. They accomplish this by maximizing a similarity metric between the tree branches and the arteries and using a series of handcrafted conditions. A non-strictly GM approach is similarly proposed by Rist et al. [67]. They perform bifurcation matching of cerebrovascular graph structures generated from vessel segmentations in order to obtain vessel labels. In more detail, they construct candidate subgraphs using a handcrafted distance measure and identify bifurcation correspondence based on a cost function iteratively evaluated on plausible vessel paths for a singular node. The collection of subgraphs is then fused according to their overlap. In a similar fashion Behkamal et al. [68] developed a GM technique that does not consider the classical GM problem, but is however included. They developed their approach for secondary structure element correspondence to cryo-electron microscopy maps in the field of bioinformatics. Briefly, features are extracted from secondary structure elements, graphs are built based on three defined mathematical based features and their respective adjacency matrices. Next, they compute the node similarities using two statistical scoring functions, obtaining possible matching sets. The final set is decided using a voting algorithm.

GM has also been used for segmentation of the whole heart great vessels including the aorta and pulmonary artery [69]. Precisely, the GM technique was used to identify the great vessels (aorta, pulmonary artery). In order to achieve this they create a graph library to resemble connections between the great and anomalous vessels. Following that, they use the graphs extracted from the segmentation, model them as distributions, and match them to the library using a similarity metric (Earth mover's distance).

Further, Rochman et al. [70] take inspiration from the work of Szeskin et al. [84] and propose a solution to the bipartite GM problem so as to obtain a correspondence between lesions in CT images as follow-up. In particular, they formulate their problem as a bipartite GM problem where vertices represent lesions and edges represent lesion matchings. In addition, they introduce connected component which define lesion changes based on their properties. The lesion correspondence is performed using greedy-overlap based coupling.

In the context of sulcal GM, Buskulic et al. [71] collected a number of two and multi-GM techniques, indicative of different classes of methods, and benchmarked their performance. Namely, the benchmark SMAC, IPFP, RRWM, KerGM [85] and mALS [86] for pair-wise and multi GM respectively. Yadav et al. [72] update this benchmark further by comparing the best performing pair-wise method (KerGM) with multi-GM methods, namely, mALS, mSync [87] and Hippi [88]. This work was further extended in [73] by adding additional multi-GM methods to compare such as MatchEig [89] and CAO [90].

IV. Discussion

In this section, we briefly discuss the methods that have been used to solve the GM problem in medical imaging and we offer some insight on the evolving methods for solving the GM problem in alternative fields. These implementations could serve as examples and have potential use in medical imaging applications, thus signalling potential future solutions for this long-studied problem.

GM has been used in a multitude of ways as demonstrated in this document. Comparison between medical imaging acquisitions is a very useful procedure in the case of diagnosis, post-operative evaluation, and intra-operative enhancement. Its correct integration in these procedures can provide abundant useful information without suffering from intra-observer variability or at least reducing its prevalence. Graph representation of data in the medical field can be very useful, stemming from the notion that medical structures can often be intuitively represented as graphs. Previous and continued work [91, 92, 93, 94] demonstrate this. Therefore, graph-based techniques, like GM, can be of great value.

In this work we separated the types of GM procedures based on the methodology employed. However, It is our firm belief that a consensus on the different categories must be reached, as the current state of research suggests that one does not exist. Different authors choose to use different categories which results in unclear categorisation of the methods and further confusion.

Our work suggests that discrete methods, spectral and continuous relaxations have all had fair share of use in medical imaging applications. Discrete methods perform adequately with the drawback of being more computationally expensive which is in some cases not within the acceptable margin for time-reliant procedures. In addition, a number of discrete methods focus on some kind of tree search method. These methods commonly assume acyclic graph structures which is rarely the case, especially in 2D vessel imaging. On the other hand, both continuous and spectral relaxations improve on the efficiency, but lack in the robustness of their results. For example, continuous methods are known to suffer from local minima and do not ensure a globally optimal solution. Despite the long on-going research, all these types of methods are still under investigation and work on their comparison is still sparse.

The evergrowing field of machine learning has demonstrated its beneficial use in medical imaging applications in a great number of ways. However, the use of machine learning and deep learning techniques for the purpose of solving quadratic problems in the medical field, such as GM, is still in its infancy. On the other hand, fields like computer vision have recently presented a plethora of methods for solving the GM problem (e.g. image matching) [13, 95, 9]. Affinity matrix learning is one of those methods and has been demonstrated several times [96, 97, 5, 98]. The basic notion revolves around the idea of learning an affinity metric given graph node embeddings, which can usually be acquired using a combination of CNN feature extraction and GNN feature embedding. In many cases these approaches are combined with the factorized affinity matrix introduced by Zhou and De la Torre [14]. A different approach sharing some similar ideas is feature matching, where the constructed node embeddings are matched [2]. An additional technique considers higher-order GM. These methods can produce results with improved robustness but are still in early development [99, 100, 101]. A number of these methods do not strictly solve the QAP but employ deep learning techniques to find correspondences. This is indicative of how deep learning techniques could potentially avoid the QAP all together and achieve improved GM results.

The vast majority of the aforementioned machine learning techniques focus on supervised methodologies. It is widely known that these approaches usually require a great number of ground truth to learn effectively. This is rarely the case in medical imaging applications as ground truth retrieval is often time consuming and impractical. Several unsupervised deep learning techniques have been proposed, but additional development is necessary [102, 103, 104, 105].

Based on the continuous development of machine learning techniques, we believe that current solutions to the GM problem will be enhanced with their use, and offer improved performance and reduced time complexity. However, the combination of problems that have a rigorous mathematical formulation with the use of machine learning techniques, typically applied on problems that do not have such a formulation, is a challenging task and their interaction should be studied thoroughly.

V. Conclusions

This paper provides a targeted survey of GM methods with a focus in medical imaging applications. It includes basic concepts, characteristic methodologies, their different variants and their application and a short discussion on possible future developments. In this review, we note the extensive use of GM techniques in medical imaging applications. Given the intuitive graph representation of human structures (e.g. vessels) and the continuous development of deep learning techniques, we expect additional GM research utilizing deep learning for medical imaging applications in the future. We believe that deep learning can enhance the performance of existing GM techniques and be invaluable, as it has been in other domains.

References

[1] J. Yan *et al.*, "A short survey of recent advances in graph matching," in *ICMR 2016 - Proceedings of the 2016 ACM International Conference on Multimedia Retrieval*, 2016, pp. 167–174. DOI: 10.1145/2911996.2912035.

[2] M. Fey *et al.*, "Deep Graph Matching Consensus," 2020.

[3] C. Oyarzun Laura *et al.*, "Graph matching survey for medical imaging: On the way to deep learning," *Methods*, vol. 202, pp. 3–13, 2022. DOI: https://doi.org/10.1016/j.ymeth.2021.06.008.

[4] A. Charnoz *et al.*, "Design of Robust Vascular Tree Matching: Validation on Liver," Tech. Rep., 2005.

[5] R. Wang *et al.*, "Combinatorial Learning of Robust Deep Graph Matching: An Embedding Based Approach," *IEEE Transactions on Pattern Analysis and Machine Intelligence*, vol. 45, no. 6, pp. 6984–7000, 2023. DOI: 10.1109/TPAMI.2020.3005590.

[6] R. K. Bhati and A. Rasool, "Quadratic Assignment Problem and its Relevance to the Real World: A Survey," Tech. Rep. 9, 2014, pp. 975–8887.

[7] L. Livi and A. Rizzi, "The graph matching problem," *Pattern Analysis and Applications*, vol. 16, no. 3, pp. 253–283, 2013. DOI: 10.1007/s10044-012-0284-8.

[8] J. Ma *et al.*, "Image Matching from Handcrafted to Deep Features: A Survey," *International Journal of Computer Vision*, vol. 129, no. 1, pp. 23–79, 2021. DOI: 10.1007/s11263-020-01359-2.

[9] H. Sun *et al.*, "A Survey on Graph Matching in Computer Vision," in *Proceedings - 2020 13th International Congress on Image and Signal Processing, BioMedical Engineering and Informatics, CISP-BMEI 2020*, 2020, pp. 225–230. DOI: 10.1109/CISP-BMEI51763.2020.9263681.

[10] B. Gallagher, "Matching Structure and Semantics: A Survey on Graph-Based Pattern Matching," in *AAAI Fall Symposium: Capturing and Using Patterns for Evidence Detection*, vol. 45, 2006.

[11] K. Riesen *et al.*, "Exact and Inexact Graph Matching: Methodology and Applications," in *Managing and Mining Graph Data*, C. Aggarwal and H. Wang, Eds., Boston, MA, 2010, pp. 217–247. DOI: 10.1007/978-1-4419-6045-0_7.

[12] D. Conte *et al.*, "Thirty years of graph matching in pattern recognition," *International journal of pattern recognition and artificial intelligence*, vol. 18, no. 03, pp. 265–298, 2004.

[13] X. Ling *et al.*, "Graph Neural Networks: Graph Matching," in *Graph Neural Networks: Foundations, Frontiers, and Applications*, L. Wu *et al.*, Eds., Singapore, 2022, pp. 277–295. DOI: 10.1007/978-981-16-6054-2_13.

[14] F. Zhou and F. De La Torre, "Factorized Graph Matching," *IEEE Transactions on Pattern Analysis and Machine Intelligence*, vol. 38, no. 9, pp. 1774–1789, 2016. DOI: 10.1109/TPAMI.2015.2501802.

[15] T. S. Caetano *et al.*, "Learning Graph Matching," 2008.

[16] J. Zhu *et al.*, "Heuristic tree searching for pose-independent 3D/2D rigid registration of vessel structures," *Physics in Medicine & Biology*, vol. 65, no. 5, p. 55 010, 2020.

[17] M. A. Pinheiro *et al.*, "Geometric Graph Matching Using Monte Carlo Tree Search," *IEEE Transactions on Pattern Analysis and Machine Intelligence*, vol. 39, no. 11, pp. 2171–2185, 2017. DOI: 10.1109/TPAMI.2016.2636200.

[18] J. Zhu *et al.*, "3D/2D Vessel Registration based on Monte Carlo Tree Search and Manifold Regularization," *IEEE Transactions on Medical Imaging*, p. 1, 2023. DOI: 10.1109/TMI.2023.3347896.

[19] S. M. Lajevardi *et al.*, "Retina verification system based on biometric graph matching," *IEEE Transactions on Image Processing*, vol. 22, no. 9, pp. 3625–3635, 2013. DOI: 10.1109/TIP.2013.2266257.

[20] R. S. Shen *et al.*, "Graph Matching Based Connectomic Biomarker with Learning for Brain Disorders," in *Lecture Notes in Computer Science (including subseries Lecture Notes in Artificial Intelligence and Lecture Notes in Bioinformatics)*, vol. 12443 LNCS, 2020, pp. 131–141. DOI: 10.1007/978-3-030-60365-6_13.

[21] G. O. Olivera *et al.*, "Using geometric graph matching in image registration," in *VISIGRAPP 2021 - Proceedings of the 16th International Joint Conference on Computer Vision, Imaging and Computer Graphics Theory and Applications*, vol. 4, 2021, pp. 87–98. DOI: 10.5220/0010239200870098.

[22] Y. Osmanlioğlu *et al.*, "System-level matching of structural and functional connectomes in the human brain," *NeuroImage*, vol. 199, pp. 93–104, 2019. DOI: 10.1016/j.neuroimage.2019.05.064.

[23] Y. Osmanlioğlu *et al.*, "Connectomic consistency: A systematic stability analysis of structural and functional connectivity," *Journal of Neural Engineering*, vol. 17, no. 4, 2020. DOI: 10.1088/1741-2552/ab947b.

[24] E. R. Olafson *et al.*, "Functional connectome reorganization relates to post-stroke motor recovery and structural and functional disconnection," *NeuroImage*, vol. 245, 2021. DOI: 10.1016/j.neuroimage.2021.118642.

[25] H. Bukhari *et al.*, "Graph-matching distance between individuals' functional connectomes varies with relatedness, age, and cognitive score," *Human Brain Mapping*, vol. 44, no. 9, pp. 3541–3554, 2023. DOI: 10.1002/hbm.26296.

[26] E. Serradell *et al.*, "Non-Rigid Graph Registration using Active Testing Search," *IEEE TRANSACTIONS ON PATTERN ANALYSIS AND MACHINE INTELLIGENCE*, 2014.

[27] E. Serradell *et al.*, "Robust elastic 2D/3D geometric graph matching," Tech. Rep., 2012.

[28] J. Garcia Guevara *et al.*, "Biomechanics-based graph matching for augmented CT-CBCT," *International Journal of Computer Assisted Radiology and Surgery*, vol. 13, no. 6, 2018. DOI: 10.1007/s11548-018-1755-1.

[29] J. Garcia Guevara *et al.*, "Elastic Registration Based on Compliance Analysis and Biomechanical Graph Matching," *Annals of Biomedical Engineering*, vol. 48, no. 1, pp. 447–462, 2020. DOI: 10.1007/s10439-019-02364-4.

[30] J. Czajkowska *et al.*, "Skeleton Graph Matching vs. Maximum Weight Cliques aorta registration techniques," *Computerized Medical Imaging and Graphics*, vol. 46, pp. 142–152, 2015. DOI: 10.1016/j.compmedimag.2015.05.001.

[31] X. Bai and L. J. Latecki, "Path Similarity Skeleton Graph Matching," 2008.

[32] S. Umeyama, "An Eigendecomposition Approach to Weighted Graph Matching Problems," *IEEE Transac-*

tions on Pattern Analysis and Machine Intelligence, vol. 10, no. 5, pp. 695–703, 1988. DOI: 10.1109/34.6778.

[33] D. Smeets *et al.*, "Robust Matching of 3D Lung Vessel Trees," Tech. Rep., 2010.

[34] K. Im *et al.*, "Quantitative comparison and analysis of sulcal patterns using sulcal graph matching: A twin study," *NeuroImage*, vol. 57, no. 3, pp. 1077–1086, 2011. DOI: 10.1016/j.neuroimage.2011.04.062.

[35] Y. Guo *et al.*, "Robust anatomical correspondence detection by hierarchical sparse graph matching," *IEEE Transactions on Medical Imaging*, vol. 32, no. 2, pp. 268–277, 2013. DOI: 10.1109/TMI.2012.2223710.

[36] H. Lombaert *et al.*, "FOCUSR: Feature oriented correspondence using spectral regularization -A method for precise surface matching," *IEEE Transactions on Pattern Analysis and Machine Intelligence*, vol. 35, no. 9, pp. 2143–2160, 2013. DOI: 10.1109/TPAMI.2012.276.

[37] M. Shakeri *et al.*, "Statistical shape analysis of subcortical structures using spectral matching," *Computerized Medical Imaging and Graphics*, vol. 52, pp. 58–71, 2016. DOI: 10.1016/j.compmedimag.2016.03.001.

[38] M. Shakeri *et al.*, "Deep Spectral-Based Shape Features for Alzheimer's Disease Classification," in *Spectral and Shape Analysis in Medical Imaging*, M. Reuter *et al.*, Eds., 2016, pp. 15–24, ISBN: 978-3-319-51237-2.

[39] R. Wright *et al.*, "Construction of a fetal spatiotemporal cortical surface atlas from in utero MRI: Application of spectral surface matching," *NeuroImage*, vol. 120, pp. 467–480, 2015. DOI: 10.1016/j.neuroimage.2015.05.087.

[40] C. Leng and H. Zhang, "The prediction of eigenvalues of the normalized laplacian matrix for image registration," *12th International Conference on Natural Computation, Fuzzy Systems and Knowledge Discovery : ICNC-FSKD*, 2016. DOI: 10.1109/FSKD.2016.7603419.

[41] G. Chen *et al.*, "Neighborhood matching for curved domains with application to denoising in diffusion MRI," in *Lecture Notes in Computer Science (including subseries Lecture Notes in Artificial Intelligence and Lecture Notes in Bioinformatics)*, vol. 10433 LNCS, 2017, pp. 629–637. DOI: 10.1007/978-3-319-66182-7_72.

[42] G. Chen *et al.*, "Denoising of Diffusion MRI Data via Graph Framelet Matching in x-q Space," *IEEE Transactions on Medical Imaging*, vol. 38, no. 12, pp. 2838–2848, 2019. DOI: 10.1109/TMI.2019.2915629.

[43] Z. Zhou and S. Hao, "Anatomical landmark detection on 3D human shapes by hierarchically utilizing multiple shape features," *Neurocomputing*, vol. 253, pp. 162–168, 2017. DOI: 10.1016/j.neucom.2016.09.131.

[44] M. Groher *et al.*, "Deformable 2D-3D registration of vascular structures in a one view scenario," *IEEE Transactions on Medical Imaging*, vol. 28, no. 6, pp. 847–860, 2009. DOI: 10.1109/TMI.2008.2011519.

[45] S. Almasi *et al.*, "Cerebrovascular network registration via an efficient attributed graph matching technique," *Medical Image Analysis*, vol. 46, pp. 118–129, 2018. DOI: 10.1016/j.media.2018.02.007.

[46] K. Deng *et al.*, "Retinal fundus image registration via vascular structure graph matching," *International Journal of Biomedical Imaging*, vol. 2010, 2010. DOI: 10.1155/2010/906067.

[47] J. H. Metzen *et al.*, "Matching of Tree Structures for Registration of Medical Images," in 2007. DOI: https://doi.org/10.1007/978-3-540-72903-7_2.

[48] J. H. Metzen *et al.*, "Matching of anatomical tree structures for registration of medical images," *Image and Vision Computing*, vol. 27, no. 7, pp. 923–933, 2009. DOI: 10.1016/j.imavis.2008.04.002.

[49] J. Liu *et al.*, "Accurate correspondence of cone photoreceptor neurons in the human eye using graph matching applied to longitudinal adaptive optics images," in *Lecture Notes in Computer Science (including subseries Lecture Notes in Artificial Intelligence and Lecture Notes in Bioinformatics)*, vol. 10434 LNCS, 2017, pp. 153–161. DOI: 10.1007/978-3-319-66185-8_18.

[50] J. Liu *et al.*, "Computer-aided detection of pattern changes in longitudinal adaptive optics images of the retinal pigment epithelium," in *Proceedings - International Symposium on Biomedical Imaging*, vol. 2018-April, 2018, pp. 34–38. DOI: 10.1109/ISBI.2018.8363517.

[51] J. Liu *et al.*, "Automated Iterative Label Transfer Improves Segmentation of Noisy Cells in Adaptive Optics Retinal Images," in *Lecture Notes in Computer Science (including subseries Lecture Notes in Artificial Intelligence and Lecture Notes in Bioinformatics)*, vol. 13003 LNCS, 2021, pp. 201–208. DOI: 10.1007/978-3-030-88210-5_19.

[52] M. Zaslavskiy *et al.*, "A path following algorithm for the graph matching problem," 2008.

[53] A. Calissano *et al.*, "Graph alignment exploiting the spatial organization improves the similarity of brain networks," *Human Brain Mapping*, vol. 45, no. 1, 2024. DOI: 10.1002/hbm.26554.

[54] S. Wang *et al.*, "Matching 3-D prone and supine CT colonography scans using graphs," *IEEE Transactions on Information Technology in Biomedicine*, vol. 16, no. 4, pp. 676–682, 2012. DOI: 10.1109/TITB.2012.2194297.

[55] C. Zhao *et al.*, "AGMN: Association graph-based graph matching network for coronary artery semantic labeling on invasive coronary angiograms," *Pattern Recognition*, vol. 143, 2023. DOI: 10.1016/j.patcog.2023.109789.

[56] C. Zhao *et al.*, "EAGMN: Coronary artery semantic labeling using edge attention graph matching network," *Computers in Biology and Medicine*, vol. 166, 2023. DOI: 10.1016/j.compbiomed.2023.107469.

[57] C. Zhao *et al.*, "Hyper Association Graph Matching with Uncertainty Quantification for Coronary Artery Semantic Labeling," 2023.

[58] R. Furukawa *et al.*, "Fully Auto-calibrated Active-stereo-based 3D Endoscopic System using Correspondence Estimation with Graph Convolutional Network," in *42nd Annual International Conference of the IEEE Engineering in Medicine & Biology Society (EMBC)*, 2020. DOI: 10.1109/EMBC44109.2020.9176417.

[59] R. Furukawa *et al.*, "Simultaneous estimation of projector and camera poses for multiple oneshot scan using pixel-wise correspondences estimated by U-Nets and GCN," *Computer Methods in Biomechanics and Biomedical Engineering: Imaging and Visualization*, vol. 10, no. 5, pp. 540–548, 2022. DOI: 10.1080/21681163.2021.2009376.

[60] M. Mikamo *et al.*, "Active Stereo Method for 3D Endoscopes using Deep-layer GCN and Graph Representation with Proximity Information," in *43rd Annual International Conference of the IEEE Engineering in Medicine & Biology Society (EMBC)*, 2021. DOI: 10.1109/EMBC46164.2021.9629696.

[61] M. Mikamo *et al.*, "GCN-Calculated Graph-Feature Embedding for 3D Endoscopic System Based on Active Stereo," in *Frontiers of Computer Vision*, H. Jeong and K. Sumi, Eds., 2021, pp. 253–266, ISBN: 978-3-030-81638-4.

[62] S. Moriconi *et al.*, "Elastic Registration of Geodesic Vascular Graphs," 2018. DOI: 10.1007/978-3-030-00928-1_91.

[63] X. Guo *et al.*, "Statistical Shape Analysis of Brain Arterial Networks (BAN)," 2022.

[64] D. Motta *et al.*, "Vessel Optimal Transport for Automated Alignment of Retinal Fundus Images," *IEEE Transactions on Image Processing*, vol. 28, no. 12, pp. 6154–6168, 2019. DOI: 10.1109/TIP.2019.2925287.

[65] J. Zhu *et al.*, "Iterative closest graph matching for non-rigid 3D/2D coronary arteries registration," *Computer Methods and Programs in Biomedicine*, vol. 199, 2021. DOI: 10.1016/j.cmpb.2020.105901.

[66] S. Riffaud *et al.*, "Automatic branch detection of the arterial system from abdominal aortic segmentation," *Medical and Biological Engineering and Computing*, vol. 60, no. 9, pp. 2639–2654, 2022. DOI: 10.1007/s11517-022-02603-2.

[67] L. Rist *et al.*, "Bifurcation matching for consistent cerebral vessel labeling in CTA of stroke patients," *International Journal of Computer Assisted Radiology and Surgery*, vol. 18, no. 3, pp. 509–516, 2023. DOI: 10.1007/s11548-022-02750-9.

[68] B. Behkamal *et al.*, "Three-dimensional graph matching to identify secondary structure correspondence of medium-resolution cryo-em density maps," *Biomolecules*, vol. 11, no. 12, 2021. DOI: 10.3390/biom11121773.

[69] Z. Yao *et al.*, "Graph matching and deep neural networks based whole heart and great vessel segmentation in congenital heart disease," *Scientific Reports*, vol. 13, no. 1, 2023. DOI: 10.1038/s41598-023-34013-1.

[70] S. Rochman *et al.*, "Graph-based automatic detection and classification of lesion changes in pairs of CT studies for oncology follow-up," *International Journal of Computer Assisted Radiology and Surgery*, vol. 19, no. 2, pp. 241–251, 2024. DOI: 10.1007/s11548-023-03000-2.

[71] N. Buskulic *et al.*, "Labelling Sulcal Graphs Across Indiviuals Using Multigraph Matching," pp. 1486–1490, 2021. DOI: 10.1109/ISBI48211.2021.9434035.

[72] R. Yadav *et al.*, "On the relevance of multi-graph matching for sulcal graphs," Tech. Rep., 2022.

[73] R. Yadav *et al.*, "Population-wise labeling of sulcal graphs using multi-graph matching," *PLoS ONE*, vol. 18, no. 11 November, 2023. DOI: 10.1371/journal.pone.0293886.

[74] A. Armiti and M. Gertz, "Vertex Similarity-A Basic Framework for Matching Geometric Graphs," Tech. Rep., 2014.

[75] X. Jiang *et al.*, *A review of multimodal image matching: Methods and applications*, 2021. DOI: 10.1016/j.inffus.2021.02.012.

[76] G. L. Scott and H. C. Longuet-Higgins, "An algorithm for associating the features of two images," *Proceedings of the Royal Society of London. Series B: Biological Sciences*, vol. 244, no. 1309, pp. 21–26, 1991.

[77] M. Leordeanu and M. Hebert, "A Spectral Technique for Correspondence Problems Using Pairwise Constraints," *Tenth IEEE International Conference on Computer Vision*, vol. 1, 2005. DOI: 10.1109/ICCV.2005.20.

[78] T. Cour *et al.*, "Balanced Graph Matching," 2006.

[79] S. Gold and A. Rangarajan, "A Graduated Assignment Algorithm for Graph Matching," Tech. Rep. 4, 1996.

[80] M. Pelillo *et al.*, "Matching Hierarchical Structures Using Association Graphs," Tech. Rep. 11, 1999.

[81] M. Pelillo, "Matching free trees, maximal cliques, and monotone game dynamics," *IEEE Transactions on Pattern Analysis and Machine Intelligence*, vol. 24, no. 11, pp. 1535–1541, 2002. DOI: 10.1109/TPAMI.2002.1046176.

[82] J. T. Vogelstein *et al.*, "Fast Approximate Quadratic programming for graph matching," *PLoS ONE*, vol. 10, no. 4, 2015. DOI: 10.1371/journal.pone.0121002.

[83] A. Nowak *et al.*, "REVISED NOTE on LEARNING QUADRATIC ASSIGNMENT with GRAPH NEURAL NETWORKS," in *2018 IEEE Data Science Workshop, DSW 2018 - Proceedings*, 2018, pp. 229–233. DOI: 10.1109/DSW.2018.8439919.

[84] A. Szeskin *et al.*, "Liver lesion changes analysis in longitudinal CECT scans by simultaneous deep learning voxel classification with SimU-Net," *Medical Image Analysis*, vol. 83, 2023. DOI: 10.1016/j.media.2022.102675.

[85] Z. Zhang *et al.*, "KerGM: Kernelized Graph Matching," in *Advances in Neural Information Processing Systems 32 (NeurIPS 2019)*, 2019.

[86] X. Zhou *et al.*, "Multi-Image Matching via Fast Alternating Minimization," in *Proceedings of the IEEE International Conference on Computer Vision (ICCV)*, 2015, pp. 4032–4040.

[87] D. Pachauri *et al.*, "Solving the multi-way matching problem by permutation synchronization," in *Advances in Neural Information Processing Systems 26*, 2013.

[88] F. Bernard *et al.*, "HiPPI: Higher-Order Projected Power Iterations for Scalable Multi-Matching," in *Proceedings of the IEEE/CVF International Conference on Computer Vision (ICCV)*, 2019, pp. 10 284–10 293.

[89] E. Maset *et al.*, "Practical and Efficient Multi-View Matching," in *Proceedings of the IEEE International Conference on Computer Vision (ICCV)*, 2017, pp. 4568–4576.

[90] J. Yan *et al.*, "Multi-Graph Matching via Affinity Optimization with Graduated Consistency Regularization," *IEEE Transactions on Pattern Analysis and Machine Intelligence*, vol. 38, no. 6, pp. 1228–1242, 2016. DOI: 10.1109/TPAMI.2015.2477832.

[91] S. Almasi *et al.*, "A novel method for identifying a graph-based representation of 3-D microvascular networks from fluorescence microscopy image stacks," *Medical Image Analysis*, vol. 20, no. 1, pp. 208–223, 2015. DOI: 10.1016/j.media.2014.11.007.

[92] S. Mishra *et al.*, "VTG-Net: A CNN Based Vessel Topology Graph Network for Retinal Artery/Vein Classification," *Frontiers in Medicine*, vol. 8, 2021. DOI: 10.3389/fmed.2021.750396.

[93] D. Drees *et al.*, "Scalable robust graph and feature extraction for arbitrary vessel networks in large volumetric datasets," *BMC bioinformatics*, vol. 22, no. 1, p. 346, 2021. DOI: 10.1186/s12859-021-04262-w.

[94] C. Prabhakar *et al.*, "Vesselformer: Towards Complete 3D Vessel Graph Generation from Images," Tech. Rep., 2023, pp. 320–331.

[95] Z. Zhang *et al.*, "Deep Learning on Graphs: A Survey," 2020.

[96] B. Jiang *et al.*, "GLMNet: Graph learning-matching convolutional networks for feature matching," *Pattern Recognition*, vol. 121, 2022. DOI: 10.1016/j.patcog.2021.108167.

[97] A. Zanfir and C. Sminchisescu, "Deep Learning of Graph Matching," *Proceedings of the IEEE Conference on Computer Vision and Pattern Recognition (CVPR)*, 2018.

[98] R. Wang *et al.*, "Neural Graph Matching Network: Learning Lawler's Quadratic Assignment Problem with Extension to Hypergraph and Multiple-graph Matching," 2019.

[99] J. Yan *et al.*, "Adaptive Discrete Hypergraph Matching," *IEEE Transactions on Cybernetics*, vol. 48, no. 2, pp. 765–779, 2018. DOI: 10.1109/TCYB.2017.2655538.

[100] J. Chen *et al.*, "HOGMMNC: A higher order graph matching with multiple network constraints model for gene-drug regulatory modules identification," *Bioinformatics*, vol. 35, no. 4, pp. 602–610, 2019. DOI: 10.1093/bioinformatics/bty662.

[101] X. Yang *et al.*, "Finding Correlated Patterns via High-Order Matching for Multiple Sourced Biological Data," *IEEE Transactions on Biomedical Engineering*, vol. 66, no. 4, pp. 1017–1025, 2019. DOI: 10.1109/TBME.2018.2866266.

[102] R. Wang *et al.*, "Unsupervised Learning of Graph Matching With Mixture of Modes via Discrepancy Minimization," *IEEE Transactions on Pattern Analysis and Machine Intelligence*, vol. 45, no. 8, pp. 10 500–10 518, 2023. DOI: 10.1109/TPAMI.2023.3257830.

[103] D. Krleza and K. Fertalj, "Graph Matching Using Hierarchical Fuzzy Graph Neural Networks," *IEEE Transactions on Fuzzy Systems*, vol. 25, no. 4, pp. 892–904, 2017. DOI: 10.1109/TFUZZ.2016.2586962.

[104] M. Leordeanu *et al.*, "Unsupervised learning for graph matching," *International Journal of Computer Vision*, vol. 96, no. 1, pp. 28–45, 2012. DOI: 10.1007/s11263-011-0442-2.

[105] Z. Liu *et al.*, "Training Free Graph Neural Networks for Graph Matching," 2022.